AD-A147 376 ICE DYNAMICS(U) COLD REGIONS RESEARCH AND ENGINEERING LAB HANOVER NH W D HIBLER JUL 84 CRREL-MONO-84-3 1/1

UNCLASSIFIED F/G 8/12 NL

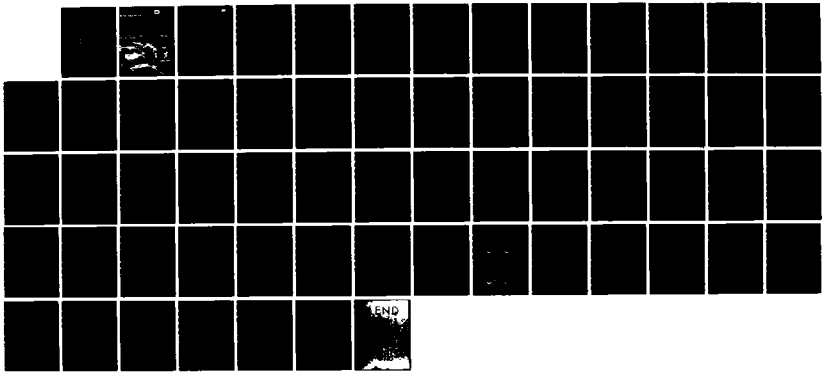

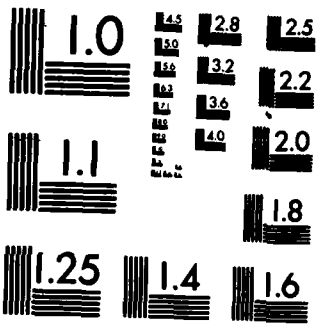
1.0
1.1
1.25
1.4
1.6
1.8
2.0
2.2
2.5
2.8
3.2
3.6
4.0
4.5
5.0
5.6
6.3

CRREL MONOGRAPH 84-3

US Army Corps of Engineers
Cold Regions Research & Engineering Laboratory

Ice dynamics

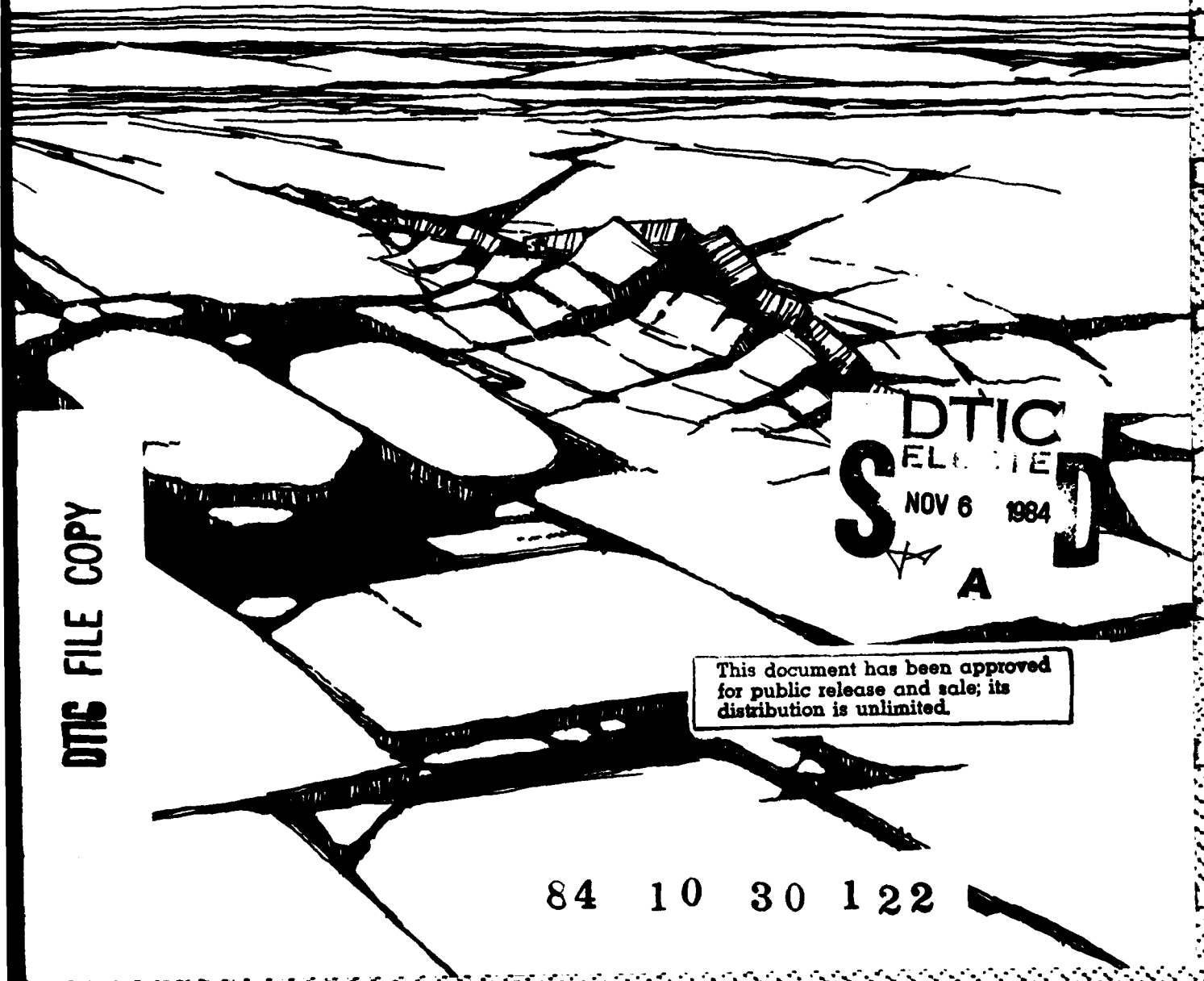

CRREL Monograph 84-3

July 1984

Ice dynamics

William D. Hibler III

Unclassified

SECURITY CLASSIFICATION OF THIS PAGE *(When Data Entered)*

REPORT DOCUMENTATION PAGE		READ INSTRUCTIONS BEFORE COMPLETING FORM
1. REPORT NUMBER Monograph 84-3	2. GOVT ACCESSION NO. AD-A147376	3. RECIPIENT'S CATALOG NUMBER
4. TITLE *(and Subtitle)* ICE DYNAMICS		5. TYPE OF REPORT & PERIOD COVERED 6. PERFORMING ORG. REPORT NUMBER
7. AUTHOR(s) William D. Hibler III		8. CONTRACT OR GRANT NUMBER(s)
9. PERFORMING ORGANIZATION NAME AND ADDRESS U.S. Army Cold Regions Research and Engineering Laboratory Hanover, New Hampshire 03755		10. PROGRAM ELEMENT, PROJECT, TASK AREA & WORK UNIT NUMBERS
11. CONTROLLING OFFICE NAME AND ADDRESS Office of Naval Research Arlington, Virginia		12. REPORT DATE July 1984 13. NUMBER OF PAGES 58
14. MONITORING AGENCY NAME & ADDRESS(if different from Controlling Office)		15. SECURITY CLASS. (of this report) Unclassified 15a. DECLASSIFICATION/DOWNGRADING SCHEDULE

16. DISTRIBUTION STATEMENT *(of this Report)*

Approved for public release; distribution unlimited.

17. DISTRIBUTION STATEMENT *(of the abstract entered in Block 20, if different from Report)*

18. SUPPLEMENTARY NOTES

Co-sponsored by NASA and the Office of Naval Research.

19. KEY WORDS *(Continue on reverse side if necessary and identify by block number)*

Arctic Ocean	Ice	Polar regions
Climate	Nonlinear mechanics	Pressure ridges
Cold regions	Oceanography	Rheology
Dynamics	Plasticity	Sea ice

20. ABSTRACT *(Continue on reverse side if necessary and identify by block number)*

This monograph reviews essential aspects of sea ice dynamics on the geophysical scale and discusses the role of ice dynamics in air-sea-ice interaction. The review is divided into the following components: a) a discussion of the momentum balance describing ice drift, b) an examination of the nature of sea ice rheology on the geophysical scale, c) an analysis of the relationship between ice strength and ice thickness characteristics, and d) a discussion of the role of ice dynamics in the atmosphere-ice-ocean system. Because of the unique, highly nonlinear nature of sea-ice interaction, special attention is given to

DD FORM 1 JAN 73 1473 EDITION OF 1 NOV 65 IS OBSOLETE

Unclassified

SECURITY CLASSIFICATION OF THIS PAGE *(When Data Entered)*

20. Abstract (cont'd)

the ramifications of ice interaction on sea ice motion and deformation. These ramifications are illustrated both by analytic solution and by numerical model results. In addition, the role of ice dynamics in the atmosphere-ice-ocean system is discussed in light of numerical modeling experiments, including a fully coupled ice-ocean model of the Arctic-Greenland-Norwegian seas.

PREFACE

This Monograph was written by William D. Hibler III, Research Physicist, Snow and Ice Branch, Research Division, U.S. Army Cold Regions Research and Engineering Laboratory. It was derived from material prepared for lectures delivered at the NATO Advanced Study Institute, October 1981, Maratea, Italy. The work was supported by the National Aeronautics and Space Administration and the Office of Naval Research.

The author thanks A. Semtner, M. Lepparanta and P. Lemke for valuable comments on the manuscript. I. Udin and A. Ullerstig provided computational aid and useful discussions on the small-scale idealized simulations. Aid in preparation of the manuscript was provided by S. Bowen and D. Harp. Computer support for small-scale simulations was provided by the Swedish Meteorological and Hydrological Institute.

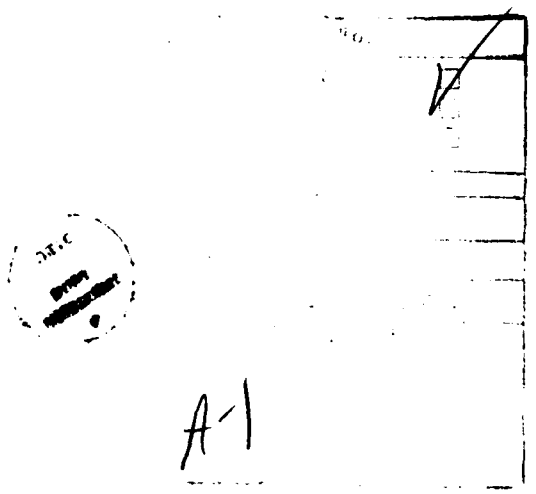

CONTENTS

ILLUSTRATIONS

TABLES

ICE DYNAMICS

William D. Hibler III

INTRODUCTION

Sea ice dynamics deals with the way momentum is transferred through the sea/ice system. The essential features of this transfer may be characterized by equations representing the following elements: 1) a momentum balance describing ice drift, including air and water stresses, Coriolis force, internal ice stress, inertial forces, and ocean current effects; 2) an ice rheology which relates the ice stress to the ice deformation and strength; and 3) an ice strength determined primarily as a function of the ice thickness distribution. In discussing these components it is implicitly assumed that a description of sea ice as a two-dimensional continuum is possible. Such a continuum description does not, however, rule out using these equations to represent rapidly changing ice conditions as occur, for example, near the ice margin. This can be accomplished by allowing various quantities (e.g. ice mass, ice strength, water stress) to vary rapidly in space. Also, most present-day treatments of ice dynamics employ highly nonlinear rheologies which can, as will be demonstrated later, introduce discontinuities into the ice velocity field, even though the forcing and mass fields may be rather smooth.

In the following review, these three elements are discussed in order. In this discussion the emphasis is on understanding the effect of ice rheology on ice drift and deformation, and both interior and ice edge dynamics are examined. The final section examines the role of ice dynamics in ice-atmosphere-ocean coupling.

MOMENTUM BALANCE

The momentum balance describes the forces that determine drift and deformation of sea ice. Denoting the ice mass per unit area by m, the momentum balance in a two-dimensional Cartesian coordinate system is

$$m D_t \underline{u} = - m f \underline{k} \times \underline{u} + \underline{\tau}_a + \underline{\tau}_w + \underline{F} - mg\nabla H \qquad (1)$$

where $D_t = (\partial/\partial t + \underline{u} \cdot \nabla)$ is the substantial time derivative, $\underline{k}$ is a unit vector normal to the surface, $\underline{u}$ is the ice velocity, f is the Coriolis parameter, $\underline{\tau}_a$ and $\underline{\tau}_w$ are the forces due to air and water stresses, H is the the dynamic height of the sea surface, and $\underline{F}$ is the force due to variations in internal ice stress. In this formulation, $\underline{\tau}_w$ is assumed to include frictional drag due to the relative movement between the ice and the under-

lying ocean. Also, H can, in principle, include the variation of the sea surface height due to atmospheric pressure changes as well as to geostrophic current balance. In this momentum balance, the air and water stresses are normally determined from idealized boundary layers, assuming constant turning angles (McPhee 1979, Brown 1980, Leavitt 1980):

$$\underline{\tau}_a = c'_a \, (\underline{U}_g \cos\phi + \underline{k} \times \underline{U}_g \sin\phi) \tag{2}$$

$$\underline{\tau}_w = c'_w [(\underline{U}_w - \underline{u}) \cos\theta + \underline{k} \times (\underline{U}_w - \underline{u}) \sin\theta)] \tag{3}$$

where $\underline{U}_g$ is the geostrophic wind, $\underline{U}_w$ the geostrophic ocean current, c'_a and c'_w air and water drag constants, and ϕ and θ air and water turning angles. In practice both the currents and the sea surface tilt are estimated from geostrophic considerations by setting H equal to the dynamic heights and computing currents by $\underline{U}_w = gf^{-1} \underline{k} \times \nabla H$, where g is the acceleration due to gravity. In general, both c'_a and c'_w are nonlinear functions of the winds winds and currents. The two most commonly used formulations are 1) linear, where c'_a and c'_w are taken to be constant, and 2) quadratic, where

$$c'_a = \rho_a \, c_a \, |\underline{U}_g| \tag{4}$$

and

$$c'_w = \rho_w \, c_w |\underline{U}_w - \underline{u}| \tag{5}$$

with c_a and c_w being dimensionless drag coefficients (with typical values of 0.0012 and 0.0055 respectively; McPhee 1980).

There are also a variety of other nonlinear boundary layer formulations, several of which have been reviewed by McPhee (1982). In some of these boundary layer models, a precise drag law cannot be specified in the form of eq 3 and 5, but rather the boundary layer characteristics are determined by the stress at the ice/water interface.

Basically, in this formulation the essential causes of the ice motion can be thought of as the geostrophic wind above the atmospheric boundary layer and the ocean current beneath the oceanic boundary layer. These forces are transmitted to the ice via simple integral boundary layers. In addition, a steady ocean current introduces a tilt (∇H) of the sea surface height (or alternatively a pressure on the ice), which also affects the ice motion. A subtle but important point with regard to the oceanic boundary layer is that there is no stress transferred from the bottom of the boundary layer to the deeper ocean. Instead, the drag upon the ice arises because of a combination of shearing and rotation in the boundary layer. This point has important ramifications for ice-ocean coupling. Specifically, while the stress transferred to the ocean is equal to the wind stress less the ice interaction, it will in general be somewhat different than the water drag on the ice. This can be seen by taking the curl of eq 1 with the internal ice force term set equal to zero. When this is done the curl of the water drag will differ from the curl of the wind stress by a term proportional to $mf\nabla\cdot u$ which arises because of the Coriolis force on the ice.

Relative magnitude of forces

With respect to the dominant components of the momentum balance, observations in conjunction with dimensional analysis show that the force balance is largely dominated by the Coriolis term, the air and water stresses, and the ice interaction. Specifically, measurements of water and air stresses show them to be of the order of 0.1 N m^{-2}. For 3-m-thick ice moving at 0.1 m s^{-1}, the Coriolis force is about 0.05 N m^{-2}, a value commensurate with the wind and water stresses. With respect to inertial force, for 3-m-thick ice, the ice must accelerate up to a typical drift rate of 0.1 m s^{-1} in less than 15 minutes to yield an inertial force of 0.1 N m^{-2}. However, the acceleration term can be significant in inertial oscillations. In this case an acceleration is induced by changing the direction of the ice motion on the same time scale as the inverse of the Coriolis parameter (about 3 hours). For most applications the momentum advection term is very small, since velocity changes of 0.1 m s^{-1} per kilometer would be needed for a 0.1 N m^{-2} force.

With respect to geostrophic current effects and the ocean tilt terms, their importance depends on the magnitude of the current fields, which are generally smaller than the ice drift rates. In the central Arctic, for example, empirical model studies (Hibler and Tucker 1979) indicate that steady current effects are normally quite small (several percent relative to the wind-driven components) for ice velocities averaged over a few days. However, even in the central basin, current and tilt effects are significant over a long time period since the wind effects tend to average out (see Fig. 1). Also, in relatively shallow regions, where barotropic effects are significant, the role of currents in ice drift may be critical.

The remaining term in the momentum balance is the ice interaction. Under typical winter conditions in the central Arctic this can be shown to be comparable to the other terms by residual calculations. A force balance obtained by Hunkins (1975) employing such a procedure is shown in Figure 2. A somewhat more direct method is to make use of the fact that in enclosed areas, such as the Bay of Bothnia, the ice does not move at all, even with significant winds (Lepparanta 1980, Omstedt and Sahlberg 1977). Based on the wind drag values discussed above this indicates ice stresses at least of the same order of magnitude as the wind and water drag. It is also possible to estimate ice stresses by considering the mechanics of the ridging process. More details on this approach and the relation of the ice interaction to the ridging process will be discussed in the section beginning on p. 23.

Free drift analysis

Much of this paper will be concerned with analyzing the effects and characteristics of the internal ice stress term F. However, it is instructive to first examine a special case of the momentum balance in which there is no ice interaction. This case is usually referred to as free drift. To further simplify matters, only steady free drift will be considered, so that the inertial terms can also be removed.

Following McPhee (1980) and Thorndike and Colony (1982) it is convenient to use complex notation to analyze this case. Writing all vectors in complex form, i.e. $\underset{\sim}{A} = Ae^{i\gamma}$, and noting that the force on the ice due to

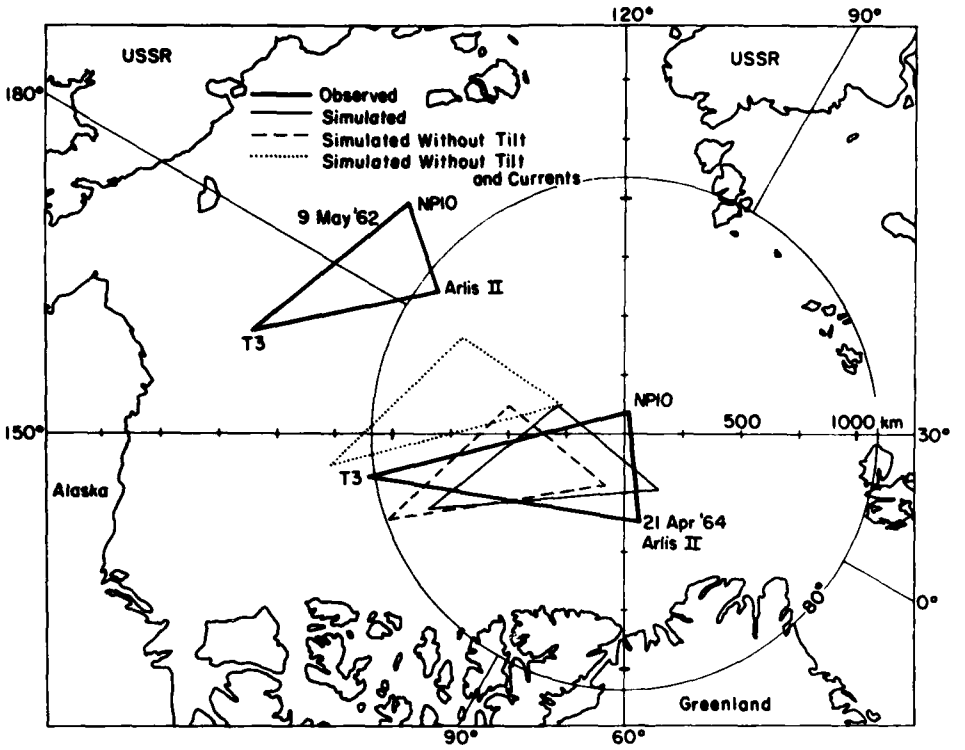

Figure 1. Simulated and observed net drift of three ice stations over a two-year period employing an empirical linear ice drift model. Simulations are shown both with and without current effects (from Hibler and Tucker 1979).

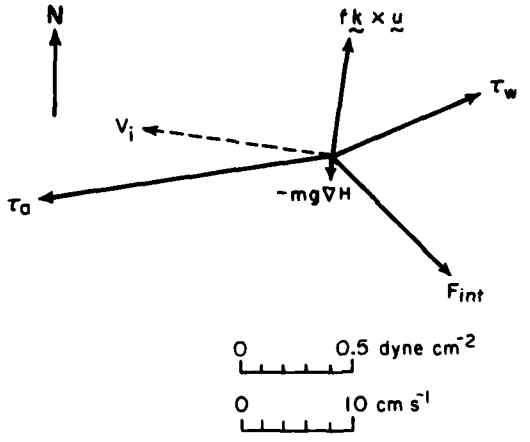

Figure 2. An estimate of the force balance on sea ice for winter conditions based on wind and water stress measurements (from Hunkins 1975). In this balance the force due to internal ice stress is determined as a residual and the dashed line shows the ice velocity.

sea surface tilt is given by $-imf\underset{\sim}{U}_w$, the steady state momentum balance can be written in the form

$$\rho_a c_a \underset{\sim}{U}_g U_g e^{i\phi} = imf\underset{\sim}{U} + \rho_w c_w \underset{\sim}{U}\, \underline{U}\, e^{i\theta} \tag{6}$$

where $\underset{\sim}{U}$ is the ice velocity relative to the steady currents:

$$\underset{\sim}{U} = \underset{\sim}{U} - \underset{\sim}{U}_w. \tag{7}$$

Letting δ be the clockwise angle from geostrophic wind to ice drift direction, eq 6 can be rewritten

$$U_g^2\, e^{i\delta} = U^2\, e^{-i\phi}\, \frac{\rho_w\, c_w}{\rho_a\, c_a}\, \left(e^{i\theta} + \frac{mf}{\rho_w c_w U}\, e^{i\pi/2}\right). \tag{8}$$

Several things are clear by inspection of eq 8. For one, if the ice mass is small enough to make the Coriolis term negligible, then the ice will drift at a rate equal to a fixed fraction of the geostrophic wind with a drift angle $\theta-\phi$ relative to the geostrophic wind. As the mass increases the ice will tend to drift further to the right of the geostrophic wind. Similar arguments also apply to the ice speed, with larger ice speeds causing the ice to drift more nearly parallel to the geostrophic wind. A final point of note is (referring back to eq 6) that for linear boundary layers, the ratio and angle between the ice drift and the wind will be fixed for a given ice mass, with increasing ice mass causing the ice to drift further to the right of the wind.

A more quantitative illustration of the nonlinear boundary layer case is given in Figure 3 which shows solutions of eq 8 in the form of ice speed and turning angle versus geostrophic wind speed for different ice masses. In this figure drag coefficients and Coriolis values similar to those used by Hibler (1979) were employed ($\rho_w = 10^3$ kg m^{-3}, $\rho_a = 1.3$ kg m^{-3}, $c_w = 0.0055$,

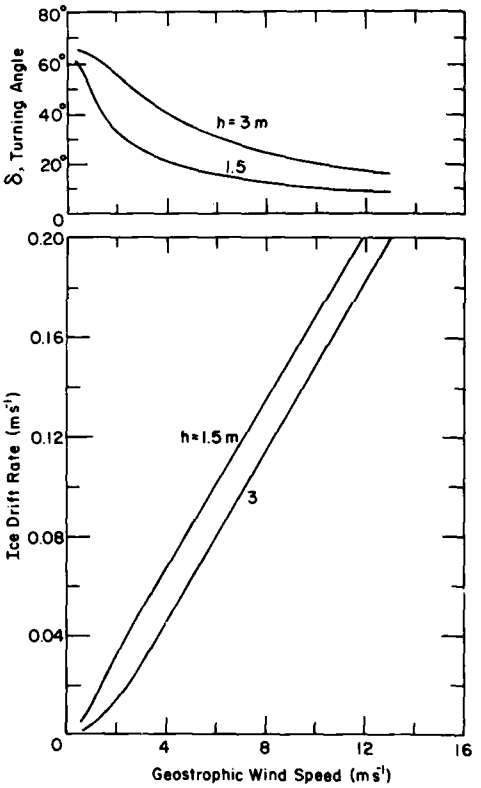

Figure 3. The ice drift rate versus the geostrophic wind speed, and the clockwise turning angle from the geostrophic wind to the ice velocity. These curves were calculated assuming free drift, and quadratic boundary layers. Curves for different ice thicknesses are shown.

$c_a = 0.0012$, $f = 1.46 \times 10^{-4}\ s^{-1}$, $\theta = \phi = 25°$). One interesting result of this plot is the very nearly linear relation between the wind speed and ice drift for all but very small speeds, despite the fact that boundary layer drags are nonlinear. This situation arises because both boundary layers are quadratic, and hence, except at low speeds, largely balance one another. However, the turning angle does show somewhat greater sensitivity to wind speed. Also note that although U and U_g are linearly related, the best linear fit does not go through the origin.

Effects of ice interaction: A qualitative discussion

It is possible to get a qualitative idea of the effect of ice interaction by examining the free drift force balance. The most obvious effect of the ice stress is to change the ice drift direction and magnitude from the free drift case. While there can be exceptions, in many cases the net effect of the ice interaction on the local force balance is to cause a force opposing the wind stress and the Coriolis force, roughly in the manner shown in Figure 4. As a consequence, to achieve the same ice velocity under these circumstances a larger wind stress more nearly parallel to the ice velocity is required.

Less obvious effects arise from the nonlinear nature of the ice interaction. As will be discussed later, over a wide range of strain rates the ice stress is expected to change relatively little. As a consequence the force due to ice stress is less sensitive to ice speed. Because of this, the modifications to free drift will become particularly pronounced at low wind speeds and ice velocities. Nonlinear interaction can also give rise to the interesting situation where, although the ice is strongly interacting, its local velocity may obey free drift. This arises because the force due to internal ice stress is given by the gradient of the ice stress, so that even though the stress is high its gradient may be very small. Because of complexities like this, high correlation of ice motion with wind fields cannot be, by itself, taken as evidence for the absence of ice interaction.

A third subtle situation which can arise due to nonlinear ice interaction is a much more "rigid body" motion of large regions of sea ice. Within the framework of a plastic rheology this state can arise where the ice stress is not large enough to exceed the plastic yield value. Under this situation the motion of the rigid body will behave very similarly to a spatially "averaged" free drift, with the main difference being that the deformation will be much different than what would be expected from free drift considerations. This particular situation is discussed in more detail in a later section.

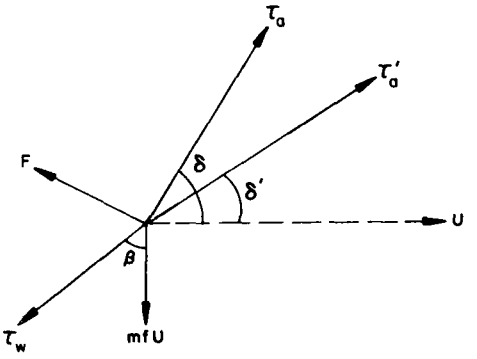

Figure 4. If the wind stress τ_a balances the water drag, Coriolis and current forces, then a larger stress τ_a', turned further to the right, is required to balance the forces with the addition of a force F due to internal ice stress.

As these general remarks indicate, the effects of ice interaction can manifest themselves in subtle and sometimes counter-intuitive ways. In the remainder of this chapter some of these subtleties will be examined in more detail.

SEA ICE RHEOLOGY

Analysis of the momentum balance has shown the importance of the internal ice stress in ice drift. Because of this, the determination of a realistic constitutive law relating the ice stress to the deformation is critical to understanding ice drift and deformation. Some of the main questions relating to ice rheologies are a) the degree of nonlinear versus linear behavior for both shearing and compressive failure, b) the relative magnitudes of shear and compressive strengths, c) the presence (if any) of an unconfined pressure term due to random bumping of floes, and d) the magnitude and dependence of ice strength on ice thickness and floe size characteristics. These questions are important for understanding the way the ice responds to external forcing and for understanding the behavior of the coupled air-ice-ocean system. In this section observational and theoretical work relating to the first three questions is discussed. The dependence and relationship of the ice strength to thickness characteristics is discussed in the next section. An attempt is made to present first a fairly unified general framework, and then to expand on the framework with various pedagogical examples employing analytical, numerical and observational work.

In discussing the rheology of sea ice it will be assumed that a description of sea ice as a two-dimensional continuum is possible. While such an approximation is reasonable, it should be remembered that pack ice does consist of individual floes, which can be as large as 20 km in the interior of the Arctic Basin and only tens of meters across near the ice margins. Because of these considerations the scale at which the continuum approximation is valid will vary. More generally, continuum motion has to be considered a statistically defined quantity for sea ice.

Theoretical framework

Considering sea ice to be a two-dimensional isotropic continuum, the most general constitutive law (see, e.g., Glen 1970, Malvern 1969) can be written in the following form:

$$\sigma_{ij} = 2\eta\dot{\epsilon}_{ij} + [(\zeta-\eta)\,(\dot{\epsilon}_{kk}) - P]\,\delta_{ij} \qquad (9)$$

where σ_{ij} is the two-dimensional stress tensor and $\dot{\epsilon}_{ij}$ the two-dimensional strain rate, $\delta_{ij} = 1$ for i equal to j or 0 for i not equal to j and η and ζ can vary spatially. In eq 9, η, ζ and P are in general functions of the two invariants of the strain rate tensor. These invariants can be taken as the principal values of ice strain rate tensor, or alternatively as $\dot{\epsilon}_{kk}$ and $\dot{\epsilon}_{ij}\,\dot{\epsilon}_{ij}$. [In these expressions and equations (and throughout this Monograph) repeated subscripts are summed over. For example $\dot{\epsilon}_{kk} = \dot{\epsilon}_{xx} + \dot{\epsilon}_{yy}$]. Within the framework of this equation, η and ζ can be thought of as nonlinear shear and bulk viscosities, while P can be viewed as a pressure term. The motivation for this nomenclature is the fact that the compres-

sive stresses and deviatoric stresses can be written as (as easily shown by manipulation of eq 9):

$$\sigma_{kk} = 2\zeta \dot{\varepsilon}_{kk} - 2P \tag{10}$$

$$\sigma'_{ij} = 2\eta \dot{\varepsilon}'_{ij} \tag{11}$$

where $\dot{\varepsilon}'_{ij} = \dot{\varepsilon}_{ij} - \dot{\varepsilon}_{kk}/2$ is the deviatoric strain rate. To obtain an internal ice force for the momentum balance, the stress tensor is differentiated:

$$F_i = \frac{\partial \sigma_{ij}}{\partial x_j}. \tag{12}$$

Particular forms of this constitutive law include both viscous and plastic rheologies. In general, a "viscous" rheology is defined as one in which stress can only be sustained through non-recoverable dissipation of energy by deformation. A "plastic" rheology, on the other hand, is one in which stress can be sustained through lack of deformation or deformation where the energy is recoverable (i.e. elastic deformation; e.g. Malvern 1969). Special cases of these rheologies often used in sea ice are a "linear viscous" rheology, where the stress depends linearly on the strain rates, and an "ideal rigid plastic" rheology, where the stress state is either indeterminate or independent of the magnitude of the strain rates. In the linear viscous case, η, ζ and P are constant. This results in a stress state linearly dependent on the strain rates. In the rigid plastic case the stress state is taken to be fixed, independent of the magnitude of the strain rate invariants, provided the ratio of the invariants does not change. In this case η and ζ will be nonlinear functions of the invariants. In the rigid plastic case, however, η and ζ are not well defined for zero strain rates. Under these conditions the ice is understood to move rigidly, with the stress determined by external balances.

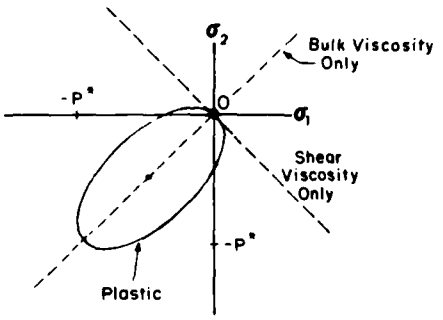

Figure 5. Allowable stress states for a linear viscous rheology with either a bulk or shear viscosity, and for an ideal rigid plastic rheology with an elliptical yield curve. The stress states are plotted as a function of the principal components of the two-dimensional stress tensor.

Some of the linear viscous and plastic rheologies proposed for sea ice are shown in Figure 5, where the allowable stress states for two particular linear viscous cases of eq 9 are shown. These states are a viscous fluid with only a shear viscosity (η = constant, $\zeta = P = 0$), and a fluid having resistance to dilation and compression but not to shear (ζ = constant, $\eta = P = 0$). For an ideal plastic constitutive law the stress state lies on or inside some fixed yield curve. In Figure 5 an elliptical yield curve is shown. For a plastic rheology a rule is needed to uniquely relate the stress state to the

strain rates. The most common rule (e.g. Malvern 1969) is to take the ratio of the strain rates for a given stress state to be that of a vector normal to the surface (this is referred to as the normal flow rule). For the ellipse, the normal flow rule yields η, ζ and P values of (see, e.g., Hibler 1977)

$$P = P^*/2 \tag{13}$$

$$\zeta = P^*/2\Delta \tag{14}$$

$$\eta = \zeta/e^2 \tag{15}$$

where

$$\Delta = [(\dot{\varepsilon}_{xx}^2 + \dot{\varepsilon}_{yy}^2)\ [1+(1/e^2)] + \frac{4}{e^2}\dot{\varepsilon}_{xy}^2 + 2\dot{\varepsilon}_{xx}\ \dot{\varepsilon}_{yy}\ (1-1/e^2)]^{1/2} \tag{16}$$

$-P^*$ is the maximum compressive stress allowable along any principal stress axis, and e is the ratio of the lengths of principal axes of the ellipse. For rigid motion, the stress state will lie within the ellipse. Note that both linear viscous laws allow large amounts of tensile strength (i.e. positive stresses), whereas this particular plastic law allows only small tensile strengths.

A general class of rheologies almost equivalent to the most general case (eq 9) has been proposed by Hibler (1979) under the name "viscous-plastic." The rheology refers to the case of eq 9 in which rigid motion does not occur, or, stated differently, any case of eq 9 in which knowledge of the strain rate uniquely specifies the stress state. This class of rheologies was proposed partly for numerical reasons and partly based on physical arguments. On the numerical side, the viscous-plastic concept is an efficient means of modeling highly nonlinear sea ice dynamics without such artifacts as elastic waves which arise in elastic-plastic simulations (Colony and Rothrock 1980). Also, the viscous-plastic approach lends itself well to formulation in a fixed Eulerian grid, which is essential for long-term seasonal simulations. On the physical side the viscous plastic rheology includes a more general class of constitutive laws than can be considered employing elastic plastic rheologies (see, e.g., Pritchard 1975). Specifically, with the viscous plastic approach it is not necessary to employ the associated flow rule. Some of these more general cases may be particularly applicable to the marginal sea ice zone.

Linear versus nonlinear behavior

A particular problem in early developments in ice dynamics was the degree of linear versus nonlinear behavior of the ice rheology. Early efforts to approximate the ice interaction made use of linear viscous models. Laikhtman (1964), for example, proposed a linear Newtonian viscous model employing only a shear viscosity, which was easy to deal with numerically and was subsequently used by a number of authors (Egorov 1970, Doronin 1970) to carry out empirical-numerical studies. The most well known application of this rheology was a calculation by Campbell (1965) of the steady circulation of the Arctic Basin using an idealized mean annual wind field. These empirical model studies demonstrated that the Newtonian viscous rheology had some ability to simulate the effects of ice interaction. How-

ever, a particular defect of this rheology is that with only a shear viscosity it has no resistance to convergence (see, e.g., Rothrock 1975a).

Empirical studies using a more "general" linear viscous law containing both bulk and shear viscosities (and hence having compressive strength, see eq 9-11) have successfully simulated observed ice drift and deformation far from shore, both over short time intervals (Hibler 1974) and over a seasonal cycle (Hibler and Tucker 1979). In particular, Hibler (1974) showed that a linear viscous rheology could explain the observation that the ice pack often tends to converge in a low pressure system in the winter and diverge in the summer under similar forcing. Best estimates of the viscosity magnitudes yielded viscosities of the order of 10^{12} kg s^{-1}, with the bulk viscosity (ζ) about twice as large as the shear viscosity (η). In a seasonal study Hibler and Tucker (1979) showed the "best fit" viscous parameters to vary in a regular seasonal manner. This seasonal variation was commensurate with the physical notion that sea ice has less thin ice in winter (due to the higher freezing rates) and hence has higher strength. The seasonal viscosity also tended to correctly simulate observed seasonal variations of the angle of ice drift relative to the wind.

However, while generally performing well far from shore, the linear viscous rheology has one major problem in that viscosities for reasonable simulations in the central pack are quite different from viscosities needed to simulate near-shore behavior (Rothrock 1975a). For example, viscosities (two-dimensional) of the order of 10^{11} to 10^{12} kg s^{-1} (Hibler 1974, Hibler and Tucker 1979) are needed to model pack ice behavior far from shore. Near shore, however, the effective viscosities may be as small as 10^{8} kg s^{-1} (Hibler et al. 1974a), and in very small channels they can be as small as 10^{5} kg s^{-1} (Sodhi and Hibler 1980). Such variations suggest that inclusion of some type of nonlinear behavior is necessary.

An additional problem with linear viscous laws is that their physical basis is questionable. In particular, the local characteristics of sea ice appear to be nonlinear and plastic in nature. However, even though sea ice may not exhibit linear viscous characterisics on a small scale, Nye (1973) has noted that such linear laws still might be appropriate for a time- or spatially averaged response. A particular case of this concept has been proposed by Hibler (1977), who suggested that on appropriate time scales stochastic fluctuations in the deformation rate might cause the average stress-strain rate relation to be essentially linear. This concept may have application to the marginal ice zone and is discussed in more detail later in this chapter.

To avoid the inherent deficiencies in linear viscous rheologies and to better describe the local real-time behavior of sea ice, Coon (1974) and Rothrock (1975a) proposed a plastic rheology for sea ice. As discussed earlier, in a plastic constitutive law the stress state of the ice is presumed to be independent of the magnitudes of the stress and strain rate. Such a law allows highly nonlinear behavior, which is helpful in explaining ice flow both near and far from shore. In addition, it contains a simple way to specify a low tensile strength concurrently with a high compressive strength. To justify such a plastic law physically, Coon and Rothrock argued that such behavior is consistent with the local physics of sea ice. The essential argument for rate independence is that the work done in ice deformation is primarily due to ridging. The energy expended in ridging,

however, would be expected to be independent of the rate of ridge building. This concept can be extended into a complete explanation (in terms of ridging and frictional losses) of all energy dissipated during plastic flow. This particular approach is discussed in the next section. With regard to small tensile strengths, it was argued that the presence (over a large scale) of many cracks prevented any effective cohesion under dilation.

While the concept of an ideal rigid plastic law is useful theoretically, it is difficult to implement in practice. In particular, to examine a plastic rheology numerically, some approximation must be made to describe the "rigid" behavior, i.e. the behavior when the ice is not flowing plastically. Two approaches have been suggested: the elastic-plastic approach (Pritchard 1975) and the viscous-plastic approach (Hibler 1979). In the elastic-plastic method the ice is assumed to behave elastically for certain strain states. The advantage of this is that it allows rigid behavior in the sense that the ice can sustain a variety of stresses while possibly undergoing no deformation. However, inclusion of the elasticity is inherently unwieldy and has the disadvantage of adding elastic waves to the behavior of the model (Colony and Rothrock 1980).

In the viscous-plastic approach (Hibler 1979), sea ice is considered to be a nonlinear viscous continuum characterized by both nonlinear bulk and shear viscosities and a pressure term. These nonlinear viscosities are adjusted to give plastic flow for normal strain rates. To close the system, for very small deformation rates the ice is assumed to behave as a very stiff linear viscous fluid. Thus the rigid behavior is approximated by a state of very slow flow. This technique is computationally advantageous. Its disadvantage, however, is that ice that is actually stationary may be modeled as slowly creeping.

Simulations using plastic rheologies have reproduced many aspects of sea ice dynamics. Near-shore simulations by Pritchard et al. (1977) have shown the capability of the elastic-plastic rheology to model both relatively stationary behavior under stress and intense shearing behavior near coasts. With respect to seasonal simulations, Hibler (1979) has shown that in addition to producing near-shore shear zone effects, a plastic rheology yields geographical ice thickness buildup and ice outflow from the Arctic Basin which agree well with observations. Also, for sufficiently high strengths, Hibler (1980a) found the modeled ice cover in the Arctic Basin stopped moving, even though the wind forcing is significant. Such a state of no motion in a constricted region, even though the external forcing is significant, is an important manifestation of a nonlinear rheology. This characteristic is a salient feature of ice drift in regions with narrow land constrictions such as the Bay of Bothnia or the Great Lakes of the United States.

Analytic analysis of a one-dimensional system

To get some feeling for the relative behavior of linear versus nonlinear rheologies and to examine the effects of nonlinear ice interaction on ice drift rates it is useful to analyze a special case of the momentum balance. Consider the one-dimensional case of the momentum balance employing only a linear water drag term cu, an external constant wind stress τ, and a one-dimensional ice interaction stress σ:

$$cu - \frac{\partial}{\partial x}[\sigma] = \tau. \tag{17}$$

Consider the region bounded by rigid walls at $x = 0$ and $x = L$. Let us now examine the linear viscous case where $\sigma = \zeta\, \partial u/\partial x$ with ζ a constant. Substituting this expression for σ into eq 17 gives

$$cu - \zeta \frac{\partial^2 u}{\partial x^2} = \tau. \tag{18}$$

A general solution of eq 18 is

$$u = A \exp\left[(c/\zeta)^{1/2} x\right] + B \exp\left[-(c/\zeta)^{1/2} x\right] + \frac{\tau}{c}. \tag{19}$$

Utilizing the boundary conditions $u(0) = u(L) = 0$ we obtain

$$u(x) = \frac{\tau}{2c\sinh(\lambda L)} \left\{\left[e^{-\lambda L} - 1\right] e^{\lambda x} + \left[1 - e^{\lambda L}\right] e^{-\lambda x}\right\} + \frac{\tau}{c} \tag{20}$$

where $\lambda = (c/\zeta)^{1/2}$.

Let us now consider a rigid plastic case with constant strength. For our plastic rheology we will assume that $\sigma = -P$ for $\partial u/\partial x < 0$ and $\sigma = 0$ for $\partial u/\partial x > 0$. These assumptions define a rigid plastic rheology with no tensile strength. A solution for this case may be constructed by noticing a) that for any deformation $\sigma = -P$ while for no motion $0 \geq \sigma \geq -P$, and b) that the maximum force would be expected to take place at the right-hand boundary since the wind stress has built up at this point. With these considerations in mind we see first that if $\tau L < P$ no motion of any kind will occur and the system will be rigid. If, on the other hand, $\tau L > P$ then a solution of eq 17 can occur for a σ satisfying the above plastic assumptions and $\sigma(L) = -P$. Integrating eq 17 from x to L we have

$$\int_x^L (cu - \tau) = -P - \sigma(x). \tag{21}$$

However, we must also have $\partial u/\partial x = 0$ except at the boundary, otherwise $\sigma(x) = -P$ and eq 17 cannot be satisfied. Therefore, u is a constant, as is τ, and we obtain

$$\sigma(x) = -P + (cu_o - \tau)(x - L). \tag{22}$$

The value of u_o may be obtained by noting that the total force acting on the rigid block moving is $-cu_oL + \tau L - P$; since there is no acceleration

$$u_o = \frac{\tau L - P}{cL}. \tag{23}$$

Another way to see this is to note that $\sigma(x=0) = 0$ since divergence is occurring there and we have assumed no tensile strength. With a little thought, this type of simple analysis can be extended to a) the equations with inertial terms (rigid block motion occurs with the block gradually speeding up to equilibrium with a spin-up time based on the water drag),

and b) a case with strong wind gradients (for sufficiently large gradients the region of convergence will occur over a finite distance rather than at a single location). In this latter case once convergence has occurred the stress will be constant, and hence free drift will occur even though the ice is interacting. These more general cases will be illustrated with some numerical examples discussed below.

This analysis is also easily extended to include nonlinear water drag terms, an extension that makes it more comparable to the free drift analysis carried out earlier in the momentum balance section. Using the notation of eq 6, the steady-state momentum balance for this one-dimensional system is

$$\rho_a c_a U_g^2 = \rho_w c_w U^2 - \frac{\partial \sigma}{\partial x}. \tag{24}$$

By the same methods as employed in the linear case for a constant wind the solution for this system is

$$U = \sqrt{\frac{\rho_a c_a U_g^2 - P/L}{\rho_w c_w}} \tag{25}$$

if $P < \rho_a c_a U_g^2 L$, and $U = 0$ otherwise. For a numerical comparison relevant to the Arctic Basin we take $L = 2.5 \times 10^3$ km, which is the scale of the Arctic Basin, and $P = 8.25 \times 10^4$ N m^{-1}, an empirical best fit ice strength for 3-m-thick ice in the Arctic Basin in winter (Hibler and Walsh 1982). Using these numbers together with the drag coefficients used in Figure 3, we obtain a comparison of free drift and drift with ice interaction as shown in Figure 6. Note that for large wind speeds there is little

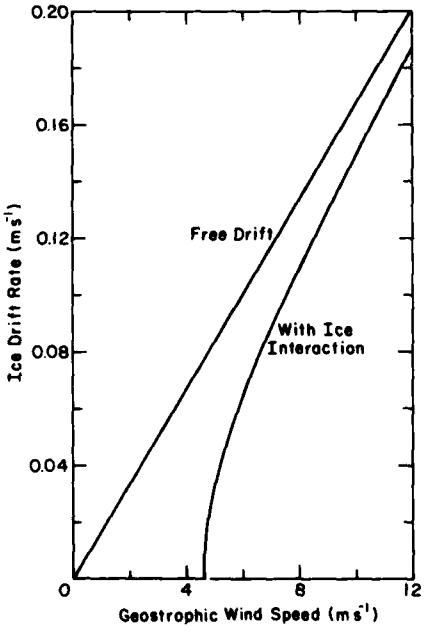

Figure 6. Comparison of ice drift rates for an idealized one-dimensional system with and without plastic ice interaction. Quadratic boundary layers were used, and for the ice interaction case typical strength and length scales relevant to the Arctic Basin were assumed. Other constants are the same as used in Figure 3 for 3-m-thick ice.

difference between free drift and the ice interaction drift whereas for smaller wind speeds the difference is very marked, with the rigid plastic system totally stopping. A significant difference from the linear water drag case is that the slope of the ice drift rate versus wind speed decreases asymptotically to the free drift slope for large geostrophic wind speeds. In the one-dimensional linear water drag case the free drift and ice interaction curves would be parallel but would have different x-axis intercepts.

A mirror reflection of this figure holds for negative ice velocities. Consequently, if one were to force this model with a zero mean Gaussian distribution of wind speeds and then fit the results with a linear model, the effect of the ice interaction would be to reduce the ratio of ice drift to wind speed. This ratio would, however, be dependent on the variance of the wind speeds, with smaller variances yielding more of a slope reduction. These considerations are relevant to linear correlations of ice drift rates with winds (Thondike and Colony 1982), which yield only slight reductions in winter. This simple analysis suggests that part of the reason for such results may be the increased intensity and hence variance of winds in winter. This analysis also indicates that although useful, such linear correlations may be masking some of the essential physics of ice drift.

Some numerical solutions for an idealized geometry

To examine the behavior of a plastic rheology for a more realistic two-dimensional geometry and for spatially varying wind forcing some numerical solutions were carried out using the viscous-plastic approach to modeling plastic flow. These solutions help verify some of the simple concepts mentioned above in the one-dimensional analysis and also demonstrate the utility of the viscous-plastic approach for modeling plastic flow.

For the momentum balance eq 1 is used with the geostrophic current U_w set equal to zero and with the momentum advection term set equal to zero:

$$m \frac{\partial \underline{u}}{\partial t} = - mf\underline{k} \times \underline{u} + \underline{\tau}_a + \underline{\tau}_w + \underline{F}. \tag{26}$$

For modeling the ice interaction the ice is considered to have a nonlinear viscous plastic constitutive law similar to that mentioned earlier.

$$\sigma_{ij} = 2\eta(\dot{\epsilon}_{ij}, P^*)\ \dot{\epsilon}_{ij} + [\zeta(\dot{\epsilon}_{ij}, P^*) - \eta\ (\dot{\epsilon}_{ij}, P^*)]\ \dot{\epsilon}_{kk}\ \delta_{ij} - P^*\sigma_{ij}/2 \tag{27}$$

where σ_{ij} is the two-dimensional stress tensor, $\dot{\epsilon}_{ij}$ the strain rate tensor, tensor, $P^*/2$ a pressure term, and ζ and η are nonlinear bulk and shear viscosities. For normal strain rates the dependences of ζ and η on $\dot{\epsilon}_{ij}$ and P^* is given by eq 13-16 so that the stress state lies on an elliptical yield curve passing through the origin with a no-stress condition applying for pure divergence. For very small strain rates the viscosities specified by eq 13-16 become arbitrarily large. To avoid this they are chosen to be the minimum of the plastic values and some large limiting values dependent on the ice strength P^*. For the calculations performed here the standard limiting values were taken to be

$$\zeta_{max} = (5.0 \times 10^7 s)P^* \tag{28}$$

$$\eta_{max} = \zeta_{max}/e^2. \tag{29}$$

Sensitivity tests (Hibler et al. 1981) show these simulation results to be relatively insensitive to these maximum viscosities unless they are taken to be about two orders of magnitude smaller. However, the maximum viscosity values do affect computational speeds, especially at finer resolution (see Hibler et al. 1981).

To solve eq 26-29 and 12-16 numerically, a time stepping procedure using finite difference techniques is employed. The computer code for this procedure was documented by Hibler (1980b). Briefly, the numerical procedure works as follows. The viscosities used in the momentum balance are based on the deformation field from the previous time step. Using these viscosities a new velocity field is obtained, a new set of viscosities are estimated, and another linearized equation solved. We will refer to each of these relaxation solutions as an "iterative time step." By carrying out several iterative time steps at each "physical time step," ideal plastic flow may be approached. In the simulations in this section 15 iterative time steps are carried out at each physical time step, so that plastic equilibrium is approached at each time step. The effect of smaller numbers of iterative time steps is discussed in more detail by Hibler et al. (1981).

Using these equations and numerical method a series of simulations over a region 148 by 148 km with fixed boundaries and fixed geostrophic wind in the x-direction were carried out (see Fig. 7). The boundary conditions consisted of specifying zero velocity at the boundaries. For later

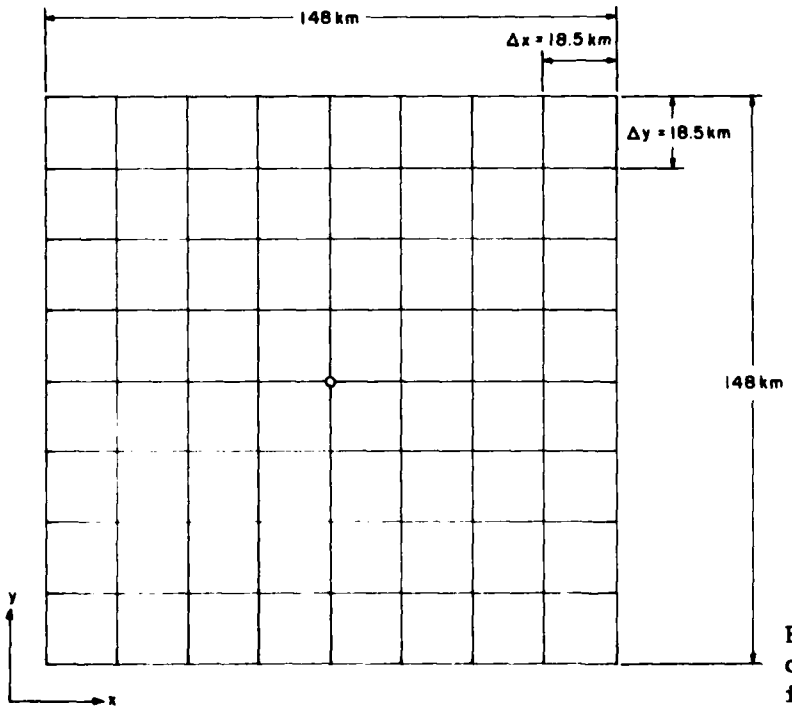

Figure 7. Boundary configuration used in idealized simulations.

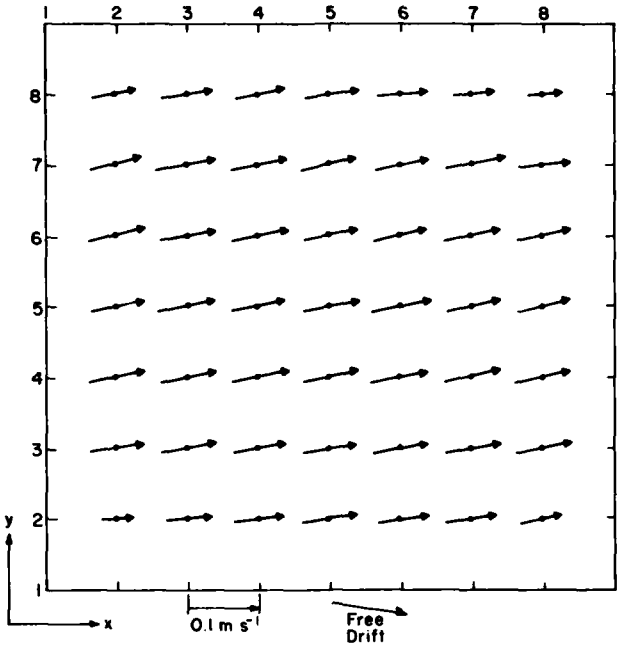

Figure 8. Equilibrium velocity field for the standard simulation.

Table 1. Numerical parameters used in standard case simulation.

$C_a = 0.0012$	$\rho_a = 1.3$ kg m^{-3}	$\Delta t = 3$ hours	$U_g = 8$ m s^{-1}
$C_w = 0.005$	$P^* = 5000$ N m^{-1}	$\zeta_{max} = (5 \cdot 10^7 s) P^*$	$V_g = 0.0$
$e = 2$	$m = 0.91 \cdot 10^3$ kg m^{-2}	$\eta_{max} = \zeta_{max}/e^2$	$U_w = 0.0$
$f = 1.46 \cdot 10^{-4} s^{-1}$	$\Delta x = \Delta y = 18.5$ km	$\phi = \theta = 25°$	$V_w = 0.0$

reference the standard simulation utilized the parameters shown in Table 1. The equilibrium velocity field for the standard simulation is shown in Figure 8. While there are some deviations due to the two-dimensional character of the rheology and boundaries this result basically represents a rigid block motion that is consistent with the simple one-dimensional arguments presented in the previous subsection. In this block motion the main converging deformation occurs at the right-hand boundary, while divergence occurs at the left-hand boundary. There is also some slight reduction of velocity at the side boundaries due to shear stresses.

Note that, as discussed above, the plastic solution is qualitatively very similar to free drift (shown in Figure 8 as a single vector ouside the grid) in that the whole sea ice region moves practically at the same velocity. However, there are quantitative differences. As in the one-dimensional case (see Fig. 6), a major difference is a smaller velocity magnitude in the plastic system than for free drift. A second significant dif-

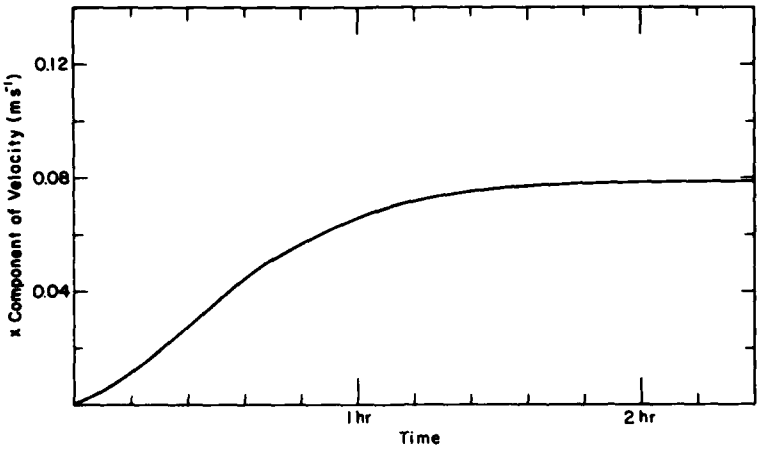

a. The component of the center point velocity versus time.

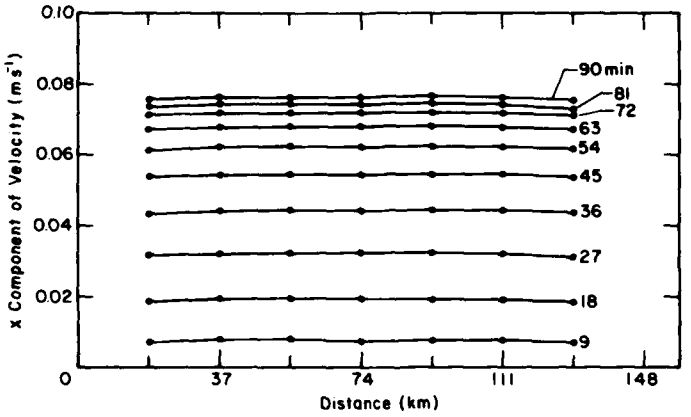

b. Profiles (taken parallel to the x axis and through the center point) of the x velocity component.

Figure 9. Inertial spin-up characteristics of idealized viscous-plastic sea ice model.

ference is a substantially reduced turning angle (15° reduction) between the plastic ice velocity vectors and the surface winds. As discussed in the earlier sections on the momentum balance (see Fig. 4) this can be explained by the fact that the force due to internal ice stress approximately opposes the ice motion. Moreover, as the ice strength increases this turning angle difference becomes even more pronounced.

The spin-up results for the standard case are shown in Figure 9. In these spin-up results 3-minute physical time steps were used as compared to 3 hours used in the other tests. Figure 9a shows the x component of the center point velocity versus time, while Figure 9b shows velocity profiles (along the x axis) at 9-minute intervals. As can be seen the spin-up is

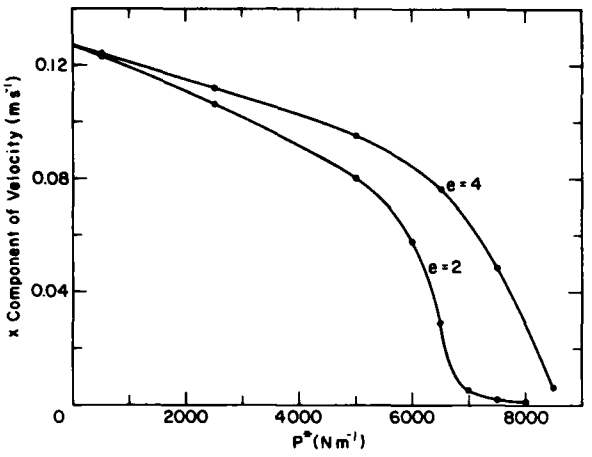

Figure 10. Equilibrium x-velocity component of the center point as a function of ice strength and for different yield curves. Curves are shown for the standard yield curve (e=2) and for a narrower elliptical yield curve with less shear strength (e=4).

also a rigid motion, with the block motion gradually increasing in accordance with the magnitude of the inertial term. A notable feature of these numerical spin-up results is that they are free of elastic wave effects that result from elastic-plastic rheologies (see, e.g., Colony and Rothrock 1980). As a result, the viscous plastic approach allows a more direct analysis of the essential physics of ice interaction with minimal numerical artifacts. Tests were also done with different strengths. Spin-up times for these cases were slightly different, due to the fact that different equilibrium velocities resulted in different water stress terms. However, with a linear water drag the spin-up times were essentially the same for different strengths.

The response of this simple system was also examined for a variety of forces of different magnitudes and having spatial variation. Analysis of the results shows that the equilibrium velocity characteristics depend on the physical size of the basin, external forcing, and ice strength. From dimensional analysis it can be deduced that near the "motion" to "no-motion" transition a key dimensionless parameter is $P^*/(\tau_a \cdot L) = \beta$, where L is the size of the region, P^* the ice strength and τ_a the wind stress. To examine the dependence on this parameter a series of tests were done with fixed resolution (Δx), size of area (L), and wind stress (τ_a). In each test a different value of P^* (fixed in time and space) was used. All other parameters were the same as the standard case. To verify the scaling, tests were also done with L and τ_a varying, with similar results as long as β was fixed. (To obtain identical results the water drag and ice mass would also have to be modified.) Figure 10 shows the component of the center point velocity versus strength from these simulations. This figure shows the strength for which the system behaves rigidly and also shows that once the strength is low enough to allow the ice to move, halving the strength brings the velocity field almost to free drift values. The value of β for the rigid "motion" to "no-motion" transition is about half of the value estimated for the one-dimensional case. This reduced value of β is primarily due to the effect of shear stress, which was not considered in the one-dimensional analysis. This hypothesis is verified in Figure 10, which shows equilibrium velocities versus P^* for a smaller ratio of shear to compressive strength (e = 4).

Figure 11 shows the effect of a spatially varying wind field. Illustrated in part a of this figure is the equilibrium ice velocity field for a wind field varying directly from 16 m s^{-1} at the left-hand boundary to zero at the right-hand boundary. As can be seen, this large velocity field gradient causes the region of rigid motion to recede to the left-hand side, with the convergence now occurring over a larger region at the right-hand side. This convergence has to occur over a band because the gradient of the stress in the rigid region now must change in order to match the external force, and the changes available for a given ice strength are limited. Figure 11b shows the case where there is an offshore wind gradient with wind varying from zero at the left-hand boundary to 16 m s^{-1} at the right-hand boundary. In this case the region of divergence is enlarged.

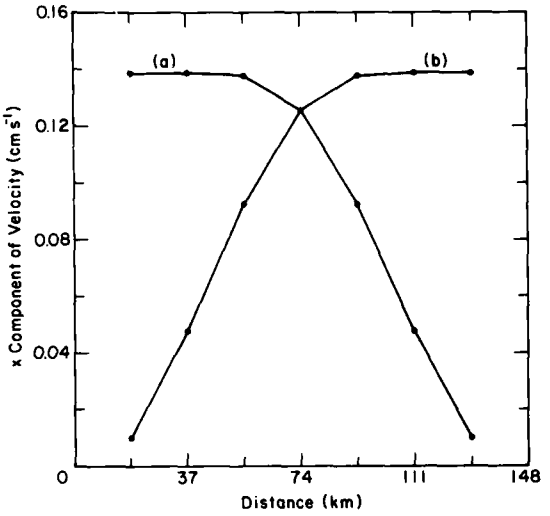

Figure 11. Effect of gradients in the wind fields on the equilibrium velocity field for the idealized domain in Figure 7. In part (a) the wind is in the positive x direction and varies from 16 m s^{-1} at the left-hand boundary to 0 at the right-hand boundary. In part (b) the wind (also in the positive x direction) starts at 0 at the left-hand boundary and goes to 16 m s^{-1} at the right-hand boundary.

An interesting feature of Figure 11 is the symmetry between the two ice drift curves for opposite gradients in the wind fields. This occurs even though the diverging ice has effectively no stress, whereas the converging ice has a stress state at the plastic yield. However, in the converging case even though the stress is large there is effectively no stress gradient and hence no significant force due to ice interaction. In general this figure demonstrates some of the counter-intuitive results that can occur with a non-linear ice interaction. In this case, even though the ice is interacting strongly the local drift still obeys free drift.

These gradient results, in conjunction with the spin-up results, have application to rapidly moving fronts. Such fronts contain large wind gradients, and on the basis of these simulations would be expected to cause moving zones of deformation to propagate ahead of the front. The block motion results also give insights into why simple free ice drift ice forecasts have generally been quite useful (see, for example, Zubov 1943). Basically, in the rigid motion case the rigid block behaves very much like freely drifting ice, except that the plastic stress tends to renormalize the wind field (or whatever external forcing exists) to a smaller value. Also, such free drift rates are usually invoked to predict the drift and not the deformation, and hence are primarily based on the smoothly varying components of the wind fields.

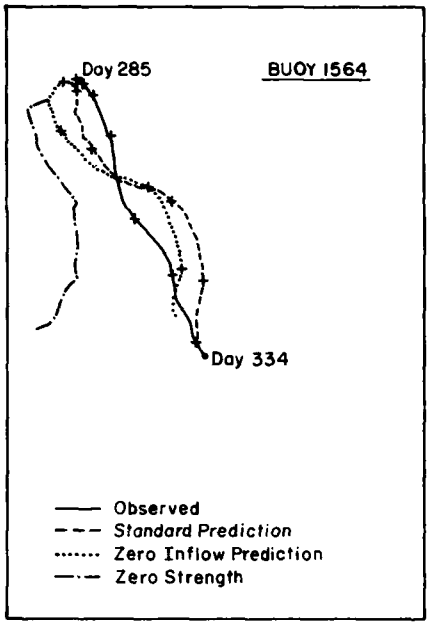

Figure 12. Simulated and observed trajectories of a buoy off East Greenland, assuming either a viscous plastic ice interaction or no ice interaction.

Stochastic effects and an unconstrained pressure term

Far from the ice edge, where the floes are large and closely packed, the ideal rigid approximation is probably good. However, near the edge there may be a great deal of random bumping of floes. This in turn may introduce an unconstrained pressure term which can do work on the continuum system. While such a rheology is still a special case of the viscous plastic rheology, it can cause a different type of ice edge dynamics than is yielded by rigid plastic analysis. However, random bumping is likely localized at the edge and will be superimposed on a larger scale behavior that has more typical plastic characteristics. Specifically, on the large scale it is likely that the ice interaction has a rectifying effect on the ice motion. Under off-ice winds, for example, the plastic nature of the ice will cause it to diverge relatively freely, whereas under on-ice winds the ice interaction will prevent further convergence.

Preliminary simulations of the East Greenland pack (Tucker and Hibler 1981) have demonstrated such a rectifying effect, and indicate that it is an important factor in the tendency of the ice to drift parallel to the coast. Figure 12, for example, shows simulated and observed trajectories for a buoy off East Greenland, assuming a viscous-plastic ice interaction. As can be seen, the ice interaction tends to prevent onshore motion of the buoy, even though the winds tend to drive it against the coast.

One way to examine the effect of random bumping and other stochastic fluctuations is to assume a plastic law locally and then average over stochastic effects in space and time. Such an approach was employed by Hibler (1977) in an attempt to relate plastic law parameters to those used in viscous models. To demonstrate the general idea let us consider the specific case of a rigid plastic law having a circular yield curve. Referring back to eq 9-16 the stress strain rate relation for such a system is:

$$\sigma_{ij} = (P^*/\Delta)\,[\dot{\varepsilon}_{ij}] - \delta_{ij}\,P^*/2 \tag{30}$$

where

$$\Delta = [(\dot{\varepsilon}_{11}^2 + \dot{\varepsilon}_{22}^2) + 4\dot{\varepsilon}_{12}^2 + 2\dot{\varepsilon}_{11}\dot{\varepsilon}_{11}]^{1/2}. \tag{31}$$

To obtain a statistical average, assume that $\dot{\varepsilon}_{ij}$ fluctuates stochastically about a mean value $\langle\dot{\varepsilon}_{ij}\rangle$ (the fluctuations could be in either time or space) with some Gaussian probability density

$$G(\dot{\varepsilon}_{ij}) = [\lambda(2\pi)^{1/2}]^{-1} \exp\,[-(\dot{\varepsilon}_{ij} - \langle\dot{\varepsilon}_{ij}\rangle)^2/2\lambda^2] \tag{32}$$

where λ is the standard deviation of the strain rate fluctuations. Consequently, the statistical average of σ_{ij}, denoted by $\langle\sigma_{ij}\rangle$, is given by

$$\langle\sigma_{ij}\rangle = [\lambda^3(2\pi)^{3/2}]^{-1} \int \exp\,\{-[(\dot{\varepsilon}_{11} - \langle\dot{\varepsilon}_{11}\rangle)^2 + (\dot{\varepsilon}_{22} - \langle\dot{\varepsilon}_{22}\rangle)^2$$

$$+ (\dot{\varepsilon}_{12} - \langle\dot{\varepsilon}_{12}\rangle)^2]/2\lambda^2\}\sigma_{ij}(\dot{\varepsilon}_{11},\dot{\varepsilon}_{22},\dot{\varepsilon}_{12})d\dot{\varepsilon}_{11}d\dot{\varepsilon}_{22}d\dot{\varepsilon}_{12} \tag{33}$$

where $\sigma_{ij}\,(\dot{\varepsilon}_{11},\dot{\varepsilon}_{22},\dot{\varepsilon}_{12})$ is given by eq 30. From this equation, two limiting cases are clear. In particular, for very small λ, which corresponds to very small fluctuations in $\dot{\varepsilon}_{ij}$, $\dot{\varepsilon}_{ij}$ in σ_{ij} may be replaced by $\langle\dot{\varepsilon}_{ij}\rangle$, in which case the plastic law is obtained for the average values. For very large λ, which corresponds to large fluctuations compared to the mean value, the right-hand side of eq 33 may be expanded in powers of $\langle\dot{\varepsilon}_{ij}\rangle/\lambda$, a procedure which would yield to first order a viscous-like law, i.e. $\langle\sigma_{ij}\rangle$ proportional to $\langle\dot{\varepsilon}_{ij}\rangle$. It is worth noting here that this expansion argument is independent of the type of distribution and constitutive law assumed. For example, considering an arbitrary constitutive law and a general probability distribution, we could still expand in powers of $\langle\dot{\varepsilon}_{ij}\rangle/\lambda$, although the actual coefficients would depend on the functional law assumed.

For the special case of a circular yield curve it is possible, by using eq 33, to estimate analytically the coefficients of the linear terms in $\langle\dot{\varepsilon}_{ij}\rangle/\lambda$. Substituting eq 30 and 31 into eq 33 and changing variables, after some algebra (see Hibler 1977), one obtains

$$\langle\sigma_{ij}\rangle = P^*\{0.35\,\langle\dot{\varepsilon}_{ij}\rangle/\lambda - 0.5\sigma_{ij}\} \tag{34}$$

where 0.35 is an approximation to two significant figures of a combination of logarithms of integers and pi. Referring back to eq 9, this expression is basically a linear viscous law with a pressure term and with $\eta = \zeta = 0.173\,P^*/\lambda$.

For the elliptical yield curve, analytic estimation of η and ζ is difficult, although their ratio can be deduced. In particular, it is clear by symmetry that in expanding eq 33 in powers of $\langle\dot{\varepsilon}_{ij}\rangle/\lambda$ the lowest-order terms will yield an average stress-strain relationship of

$$\langle \sigma_{ij} \rangle = 2\eta \langle \dot{\sigma}_{ij} \rangle + (\zeta - \eta) \langle \dot{\varepsilon}_{kk} \rangle \delta_{ij} - \delta_{ij}/2P^* \tag{35}$$

where $\zeta/\eta = e^2$. Consequently, as the ellipse becomes more elongated, the ratio ζ/η will increase.

For a more specific application of this concept one can consider the case of fluctuation in time of the deformation at a given location. Using observed and simulated deformation results, Hibler (1977) was able to show that averaging over a period of only a few days yielded a more linear-like behavior, together with a finite pressure term. Considering other effects, such as inertial oscillations that are probably prominent near the edge, it is likely that necessary averaging intervals for these stochastic arguments will be quite small, and likely shorter than typical temporal wind variations.

The ramifications of such a pressure term and nonlinear behavior near the edge are not clear. However, one interesting case has been investigated by Roed and O'Brien (1981). They considered the case of an unconstrained pressure term only, without shear strength of any kind, and without water drag. When this rheology was coupled to a Coriolis force and to a simple continuity equation for the ice compactness, geostrophic adjustment tended to cause a jet-like effect to appear at the ice edge. While this calculation is a bit unrealistic it is suggestive of some of the rheology-induced phenomena that may occur near the ice edge.

Relative magnitudes of shear and compressive strengths

The above stochastic arguments give some justification for using linear viscous laws in certain circumstances. One example of such a calculation is an idealized infinite boundary calculation performed by Hibler (1974). The main reason for this calculation was to compare observed deformation models. However, the calculations also give some insight into the relative magnitudes of shear and compressive strengths. Specifically, these idealized calculations yield a best fit bulk viscosity about twice as large as the shear viscosity. This in turn suggests that although of the same order of magnitude, compressive strengths are likely larger than shear strengths.

The basic idea in the calculation was to consider a linearized momentum balance (linear air and water drag) employing a linear constitutive law

$$\sigma_{ij} = 2\eta \dot{\varepsilon}_{ij} + (\zeta - \eta)\, \dot{\varepsilon}_{kk}\, \delta_{ij}. \tag{36}$$

Solving these equations in the case of an infinite boundary, and taking the limit of large viscosities, yielded the result that the divergence rate over the vorticity is given by

$$\frac{\nabla \cdot \underline{u}}{\mathbf{k} \cdot \nabla \times \underline{u}} = -\tan\phi \, \frac{2\eta}{(\eta + \zeta)} \tag{37}$$

where ϕ is the turning angle of the atmospheric boundary layer. Comparison of observed ice vorticity and divergence rate over a month-long period (see

Hibler 1974) did show a negative correlation, with the vorticity being about twice as large as the divergence rate. This in turn indicated that $\zeta \approx 2\eta$ and suggests that the compressive strength is larger than the shear strength.

RELATION OF ICE STRENGTH TO ICE THICKNESS CHARACTERISTICS

In the above studies we have discussed the behavior of ice dynamics under conditions where a constant strength is specified. However, in practice the ice strength is related to ice thickness characteristics in some way. To approximate the concept there have been two general approaches to date: a multi-level approach developed by Thorndike et al. (1975) and a two-level approach developed by Hibler (1979). In the multi-level approach the ice thickness distribution is broken down into a large number of levels and the strength determined by a hypothesized model of the ice ridge building process. In the two-level approach the ice strength is empirically related to the compactness and the mean ice thickness. In the next two subsections we discuss these approaches. In the first section a critique of the Thorndike et al. (1975) ridge building process is presented, and other redistributors are presented and discussed. This section also gives estimates of ice strength based on mechanical considerations and compares these strengths to best fit strengths used in numerical simulations to obtain agreement with observed drift. The two-level formulation of ice strength is discussed in the second subsection. A brief comparison of one-year simulations of the Arctic Basin ice cover employing the multi-level and two-level formulations is given in the third subsection. Finally, in the fourth subsection some of the small scale ramifications of a nonlinear coupling between ice strength and ice thickness characteristics are discussed.

Variable thickness parameterization of ice strength

Recent work on the strength of a variable thickness ice cover has been largely based on the concept, first suggested by Parmerter and Coon (1972) in a kinematic ridge model, that the major work done in ridge building is due to potential energy changes caused by ice pile-up. Rothrock (1975b) followed up this idea by suggesting that this concept be extended to two dimensions by insisting that two-dimensional deformational work be explicitly related to the amount of work done by ridging. However, if one accepts this hypothesis it then becomes critical to determine how ice ridges.

To formulate the ridge building process on the geophysical scale Thorndike et al. (1975) suggested that thin ice be redistributed into thicker ice categories. The precise manner in which this redistribution should be carried out is not clear. As an initial guess, Thorndike et al. (1975) suggested a redistributor which transfers ice into categories that are fixed multiples of the initial thickness. Ridge observations and theoretical considerations suggest that such a redistributor is unrealistic. In order to provide a more realistic parameterization of the ridging process, Hibler (1980a) proposed a scaling law for ridge building, and used this scaling law in a seasonal equilibrium simulation of the Arctic Basin ice cover. In the discussion below we examine in more detail the strength characteristics of different redistribution processes, and compare these

processes to ridge morphological data. In addition, annual ridge build-up results from the seasonal equilibrium simulation of Hibler (1980a) are reported and compared to observations of ice roughness.

General framework. Following Thorndike et al. (1975) the ice thickness characteristics are described by an areal ice thickness distribution g(h,x,t), where g(h,x,t)dh is the fraction of area (in a region centered at position x at time t) covered by ice with thickness between h and h + dh. This distribution evolves in response to deformation, advection, growth and decay. Neglecting lateral melting effects Thorndike et al. (1975) derived the following governing equation for the thickness distribution:

$$\frac{\partial g}{\partial t} + \nabla\cdot(\underline{u}g) + \frac{\partial(fg)}{\partial h} = \psi \tag{38}$$

where f is the vertical growth (or decay) rate of ice of thickness h and ψ is a redistribution function (depending on h and g) that describes the creation of open water and the transfer of ice from one thickness to another by rafting and ridging. In general, f is considered to be a function of g(h), and ψ a function of both g(h) and the rate of deformation. Except for the last two terms, eq 38 is a normal continuity equation for g. The last term on the left-hand side can also be considered a continuity requirement in thickness space since it represents a transfer of ice from one thickness category to another by the growth rates. An important feature of the Thorndike et al. (1975) theory is that it presents an "Eulerian" description in thickness space. In particular, growth occurs by rearranging the relative areal magnitudes of different thickness categories.

This equation can be formally generalized (Hibler 1980a) to include lateral melt by simply adding a source and sink term $F_L(g,h)$, such that

$$\int_0^\infty F_L dh = 0. \tag{39}$$

Equation 39 follows from the fact that, by definition, lateral melting of ice will be compensated for by a change in the extent of open water. In addition, $F_L > 0$ for $h = 0$ and $F_L < 0$ for $h > 0$. These conditions reflect the fact that lateral melting decreases the areal extent of ice while increasing open water extent. Adding this lateral growth term to eq 38, the more general thickness distribution equation becomes

$$\frac{\partial g}{\partial t} + \nabla\cdot(\underline{u}g) + \frac{\partial(fg)}{\partial h} = F_L + \psi. \tag{40}$$

Mechanical redistributor. Consider now a two-dimensional continuum with ice described by a plastic rheology such that the stress state $\sigma_{ij}(\dot{\varepsilon}_{ij},P^*)$ is a function of the strain rate $\dot{\varepsilon}_{ij}$ and a strength P*. Then, following Thorndike et al. (1975) and Rothrock (1975b), the mechanical redistribution function ψ can be reasonably postulated to satisfy the constraints

$$\int_0^\infty \psi dh = \nabla\cdot\underline{u} \tag{41}$$

$$\int_0^\infty h\psi dh = 0 \tag{42}$$

$$C \int_0^\infty h^2 \psi(h) dh = \sigma_{ij} \dot{\varepsilon}_{ij} \tag{43}$$

where $\underline{u}$ is the ice velocity field and C a constant. Considering only the work done on the ice by gravitational and buoyancy forces, C would be given by

$$C_b = \frac{1}{2} \rho_I \left[\frac{\rho_w - \rho_I}{\rho_w}\right] g \tag{44}$$

with ρ_I the density of ice, ρ_w the density of water, and g the acceleration due to gravity. Equation 41 follows from the constraint that ψ renormalizes the g distribution to unity due to changes in area. Equation 42 follows from conservation of mass and basically states that ψ does not create or destroy ice but merely changes its distribution. (An additional assumption in eq 42 is that the ice mass is related in a fixed manner to the thickness.) The third constraint (Rothrock 1975b) specifies that work done in building ridges is equal to the deformational work. An important feature of this constraint is that, for an arbitrary plastic yield curve, it forces some ridging to occur even though there may be no net convergence. In its present form (with $C = C_b$) eq 43 ignores frictional losses occurring in ridging and considers only the potential energy change due to deformed ice being lifted against gravity and being forced down against buoyancy. However, Rothrock (1975b) has estimated these frictional losses to be the same order of magnitude as the potential energy changes. Consequently, as a crude approximation for frictional losses, eq 43 is retained here with a constant C equal to $2C_b$.

A redistribution which satisfies these constraints is (using the convention that repeated subscripts are summed over)

$$\psi = \delta(h)[(P^*)^{-1} \sigma_{ij} \dot{\varepsilon}_{ij} + \dot{\varepsilon}_{kk}] + (P^*)^{-1} \sigma_{ij} \dot{\varepsilon}_{ij} W_r(h,g) \tag{45}$$

where $\delta(h)$ is the dirac delta function and

$$W_r(h,g) = \frac{[-P(h)g(h) + \int_0^\infty \gamma(h',h)P(h')g(h')dh']}{\int_0^\infty [P(h)g(h) - \int_0^\infty \gamma(h',h)P(h')g(h')dh']dh} . \tag{46}$$

The first term in eq 45 specifies the amount of open water created, while the second term describes the transfer of thin ice to thicker categories by ridging. In this formalism $\gamma(h_1,h_2)dh_2$ can be thought of as the area of ice put into the thickness interval $[h_2, h_2 + dh_2]$ when a unit area of ice of thickness h_1 is used up. Basically the integral over γ specifies where the ice is transferred to during ridging. The function P(h), on the other hand, is some probability function specifying which categories are being destroyed by ridging. Written in this form ψ automatically satisfies eq 41. To satisfy eq 42 and 43 leads to the additional constraints, respectively,

$$\int_0^\infty \gamma(h',h)h\,dh = h' \tag{47}$$

$$C \int_0^\infty W_r h^2 dh = P^*. \tag{48}$$

Equation 47 requires that transfer of ice from one category to another does not change its mass, and eq 48 serves as a definition of ice strength P^*.

The two main unknowns in the redistribution theory of ridging are $P(h)$ and $\gamma(h_1,h_2)$. Thorndike et al. (1975) have suggested that $P(h)$ be given by

$$P(h) = \max\left[\left(1 - \int_0^h g(h)dh/c_1\right),0\right] \tag{49}$$

where c_1 is a constant, say 0.15. The basic idea here is that under ridging conditions the closure of both thin ice and thick ice occurs. However, the thinnest ice is allowed to be removed to a greater extent. By fixing c_1 to be 0.15, only the thinnest 15% of the ice is deformed. Note that if there is, say, 25% open water, only open water will be removed and no ridging will occur.

The other unknown is $\gamma(h_1,h_2)$, which specifies how ice is transferred from one category to another by ridging. Thorndike et al. (1975) have suggested that

$$\gamma(h_1,h_2) = \delta(h_2 - Kh_1)K^{-1} \tag{50}$$

where K is a constant. Equation 50 effectively states that ice is transferred into a fixed multiple of its own thickness. This form is computationally simple and is useful for examining the behavior of the ice thickness distribution model.

However, the redistribution of eq 50 ignores two important physical features of the ridging. One feature is that under deformation, ridging transfers ice to a variety of thickness categories. This, for example, is evident from field observations of ridges (see, e.g., Weeks et al. 1971, Kovacs 1972), which show them to be roughly triangular. These observations indicate that under deformation, leads containing thin ice of a given thickness typically form ridges having a triangular cross section. To satisfy eq 50 such ridges would have to have vertical sides.

The second physical feature is that typical ridge heights divided by the thickness of ice being ridged appear to decrease with increasing thickness (see, e.g., Tucker and Govoni 1981). This particular scaling is an important feature of the Parmerter and Coon (1972) mechanistic ridge model. In particular, Parmerter and Coon (1972) found that simulated ridges using their mechanistic model tended to have a maximum limiting height. This limiting height, however, tended to increase more slowly than the thickness of ice being ridged.

To avoid some of these shortcomings Hibler (1980a) proposed a redistributor which distributed ice over a variety of thickness categories and, perhaps more importantly, the limiting height was taken to scale as the square root of the thickness of ice being ridged. Hibler (1980a) further

noted that such a square root dependence is consistent with one's intuition concerning ridging. Consider, for example, two equal width leads undergoing ridging. Assuming that all the thin ice is deformed into piles of relatively small blocks with similar slope angles, the two ridges formed would have heights scaling with the thickness of ice being ridged. If the distribution of lead widths is independent of the ice thickness in leads, such an intuitive argument should have application.

A comparison of redistributors. To examine the ramification of different redistributors let us compare eq 50 to several other forms for $\gamma(h_1,h_2)$ that have been suggested, or are introduced here for pedagogical purposes:

Redistribution	Eq	Description
$\gamma(h_1,h_2) = \delta(h_2-Kh_1)\frac{1}{K}$	(51)	Thorndike et al. (1975)
with K = constant		
$\gamma(h_1,h_2) = \frac{1}{2(H^*-h_1)}$ for $2h_1 \leq h_2 \leq 2\sqrt{H^*}\sqrt{h_1}$	(52)	Hibler (1980a)
with H* = constant		
$\gamma(h_1,h_2) = \frac{2}{h_1(K^2-4)}$ for $2h_1 \leq h_2 \leq Kh_1$	(53)	Modified Hibler (1980a)
with K = constant		
$\gamma(h_1,h_2) = \delta(h_2-H')\frac{h_1}{H'}$	(54)	Rubble redistribution

The scaling characteristics of different redistributors can be tested by field examination of ridge height and block size characteristics. A particularly useful data set for this purpose has been obtained and analyzed by Tucker and Govoni (1981). This data set was taken off the North Slope of Alaska. Figure 13 shows the salient characteristics of the data set

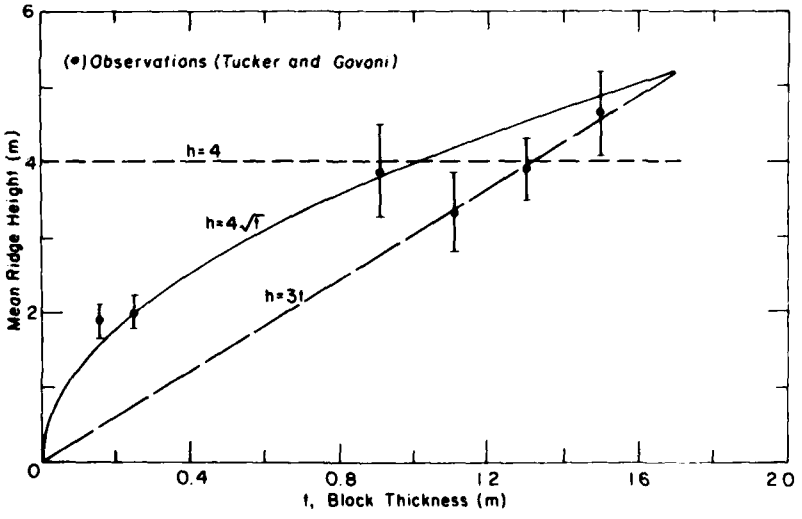

Figure 13. Comparison of different redistribution scaling laws with observed data. The solid curve represents the Hibler (1980) scaling (eq 52), the large dashed curve the Thorndike et al. (1975) scaling (eq 51), and the small dashed curve the "rubble" scaling.

relevant to the redistribution theory. The error bars are the standard error in the mean ridge height estimate. As can be seen from this figure the square root scaling fits these limited data better.

To approximately convert the ridge height scaling to an ice thickness scaling, a 4:1 ridge keel to sail ratio is assumed (Kovacs and Mellor 1974). With this scaling the square root case is equivalent to an H* of 100 m in the Hibler redistributor, whereas the linear scaling represents a modified Hibler redistributor. The rubble case represents a fixed thickness H' = 20 m.

Of particular relevance to ice mechanics are the ice strengths generated by different redistributors. To get some feeling for these strengths, consider the special case of only one thickness of ice, say h_o, being ridged. Formally representing this condition by $P(h) = \delta(h-h_o)$ one can substitute eq 46 in eq 48 and obtain analytical results for the ice strength. After some algebra different redistributors yield the following strength equations:

$$P^* = \frac{Ch_o^2 \quad (4\Gamma^3 - 3\Gamma^2 - 1)}{3(\Gamma-1)\ \Gamma} \tag{55}$$

where $\Gamma = \sqrt{H^*/h_o}$ for the Hibler redistributor and $\Gamma = K/2$ for the modified Hibler case,

$$P^* = Ch_o^2 K \tag{56}$$

for the Thorndike et al. (1975) redistribution,

$$P^* = Ch_o H' \tag{57}$$

for the rubble redistributor.

Using a representative value for C of 0.8026×10^3 N m^{-3} the various scalings in Figure 13 yield the strength versus thickness results shown in Figure 14. In the constant maximum cutoff case we have used the modified Hibler redistributor. However, from the above strength equation it is clear that the Thorndike et al. (1975) definition would give about the same strength versus thickness variation, but with all strengths 50% larger than the modified Hibler (1980a) redistributor.

The main feature illustrated by Figure 14 is that as expected the square root scaling tends to give higher strengths for thinner ice than the constant scaling. The reverse is true for thick ice. However, in both these cases the three-dimensional stress will increase as the ice becomes thicker. This is in contrast to the rubble case where the three-dimensional stress will be a constant at $\sim 1.6 \times 10^4$ N m^{-2} (or 2.3 psi).

Selected seasonal numerical results. The Hibler (1980a) redistributor (eq 52) has been used as one component of a coupled variable thickness dynamic thermodynamic sea ice model. This model has been used to carry out a seasonal equilibrium simulation of the Arctic Basin ice cover by integrating the model for five years with the same seasonal forcing being repeated each year. Of particular interest to this review are the ridge buildup results and the sensitivity of the model to different assumed frictional energy dis-

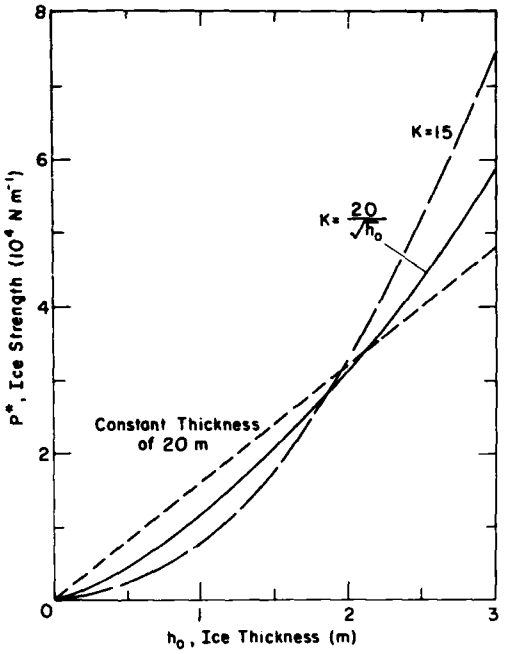

Figure 14. Ice strength versus thickness for different redistributors. The solid and long-dashed lines are for a uniform redistribution with the maximum thickness scaling as the square root (long-dashed line) of the thickness of ice being ridged (eq 52), and linearly (solid line) with the thickness of ice being ridged (eq 51 and 53). The short-dashed line is for the "rubble" redistributor (eq 54) where all ice is transferred into a 20-m thickness. In these curves, frictional losses are assumed to be equal to changes in gravitation potential energy.

sipation values in the ridging process. With regard to ridge buildup, while the model does not explicitly keep track of ridging it is possible to determine the volume of deformed ice created over an annual cycle at a fixed location. Figure 15 shows fifth-year contours of this quantity using the H* value of 50 m in eq 52 and a C value in eq 48 of $2C_b$ (see eq 44). The general shape of the roughness contours agrees well with surface roughness observations in the western Arctic Basin (Weeks et al. 1971, Hibler et al. 1974). The two major features are a heavy buildup of ridging off the Canadian Archipelago and less ridging in the Beaufort Sea than near the pole. Note, however, that there is a zone of heavy ridging just off the North Slope, in agreement with observations by Tucker et al. (1979). (This feature is masked in Figure 15 by the large contouring interval. Finer contouring intervals show a peak in the volume of deformed ice per unit area between the two 0.2-m contours in Figure 15 off the North Slope.) The other major feature is a tongue of high ridging further offshore near the tip of Greenland. Roughness data obtained from submarine sonar profiles by LeShack (private communication) also show such a tongue.

With regard to ice strengths on the geophysical scale, a major unknown factor is the amount of frictional energy loss occurring during ridging. To get an estimate of how increases in this assumed frictional loss affect drift simulations, Hibler (1980a) also carried out a sensitivity study with the frictional energy losses assumed to be 9 times the potential energy change ($C = 10\ C_b$). This high strength case resulted in an unrealistic stoppage of flow in April and May in the Arctic Basin. With the frictional loss equal to the potential energy change, on the other hand, excessively large ice drifts were obtained. Some of the differences between these two simulations are illustrated in Table 2 which compares average net simulated drift of three ice stations obtained during a 335-day period of the simulation. The simulated net drift values were obtained by interpolating ice velocity vectors to the location of the ice stations on each day and then

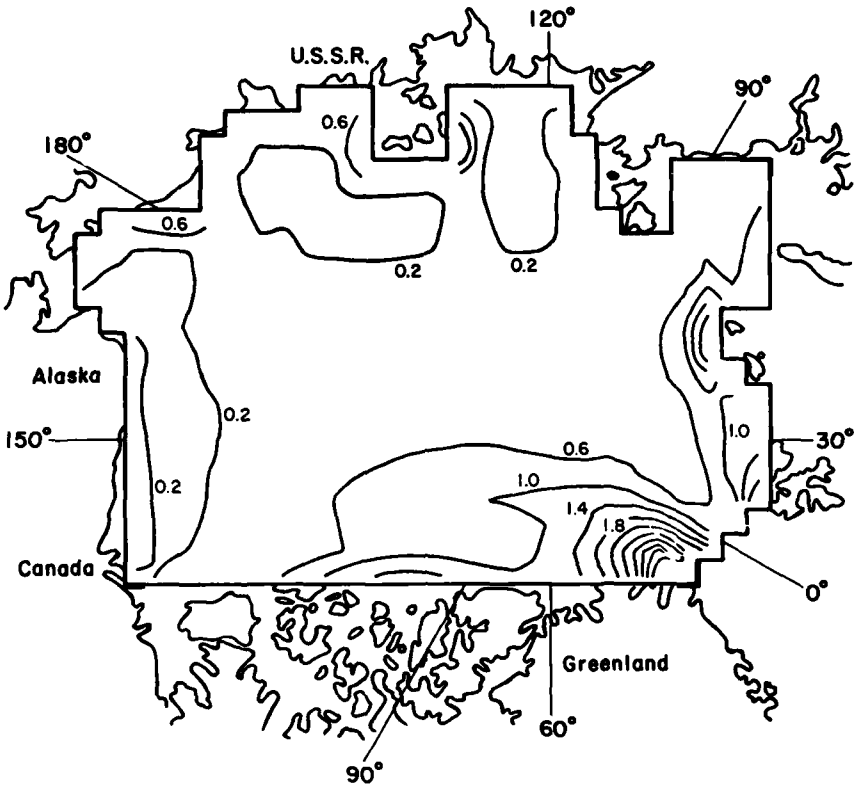

Figure 15. Contours (in meters) of simulated volume of deformed ice per unit area for one annual cycle. In the simulation a ten-level ice thickness distribution was used in conjunction with a viscous-plastic rheology. A description of the model is given by Hibler (1980).

Table 2. Observed and simulated ice station drift.

	Standard simulation ($C = 2C_b$)	High strength ($C = 10\ C_b$)	Observed
Net ice station drift	702 km	339 km	562 km
Net drift angle	26° W	13° W	6° W

multiplying by the total time. In addition to changing C, it is also possible to increase the strengths by increasing H* (see eq 46). With respect to maximum P* values near the pole in these two simulations, the high strength case yielded a maximum P* value of about 7×10^4 N m^{-1}, whereas the standard case yielded a maximum P* of about 1×10^4 N m^{-1}. Both these maxima occurred in March.

Two-level formulation of ice strength

The multi-level parameterization provides a consistent way of treating a variable thickness ice cover. However, as is apparent from the above discussion it tends to transfer much of the complexity of the problem to

the mechanical redistribution function, which is rather complicated and inherently contains a number of assumptions. The idea in the two-level approach (Hibler 1979) is to approximate the whole thickness distribution by two categories of ice: thick and thin. When this is done the treatment of the ridging process becomes much simpler. The strength is then taken to be an empirical function of these two categories, with the most important strength dependence being on the thin ice. This empirical function does contain some assumptions, but as discussed above the mechanical redistribution function also contains a large number of assumptions. Also, a two-level arctic sea ice simulation discussed in the next section yields results for ice thickness and drift in the Arctic Basin very similar to those obtained from the multi-level model, which indicates that for many climatic studies the two-level approach may be quite useful.

The basic concept in the two-level approach is that many of the dynamic and thermodynamic characteristics of sea ice are dominated by the thin ice. Consequently, for many purposes the ice thickness distribution may be approximately characterized by breaking it into two parts (thick and thin). The idea here is that if the thin ice component is monitored, then uncertainties in the remaining ice thickness distribution may not be critical. Within this two-level approach the ice cover is broken down into an area A (often called the compactness), which is covered by thick ice, and a remaining area 1-A, which is covered by thin ice, which, for computational convenience, is always taken to be of zero thickness (i.e. open water). The idea here is to have the open water approximately represent the combined fraction of both open water and thin ice up to some cutoff thickness h_0. The remainder of the ice is distributed arbitrarily. However, since the thin ice mass is normally small, the mean thickness of the remaining "thick" ice is approximately equal to h/A.

For the mean thickness h and compactness A the following continuity equations are used:

$$\partial h/\partial t = -\partial(uh)/\partial x - \partial(vh)/\partial y + S_h \tag{58}$$

$$\partial A/\partial t = -\partial(uA)/\partial x - \partial(vA)/\partial y + S_A \tag{59}$$

where $A < 1$, u is the x component of the ice velocity vector, v the y component of the ice velocity vector, and S_h and S_A are thermodynamic terms. While eq 58 is a simple continuity equation for ice mass (characterized by the mean thickness h), with thermodynamic source and sink terms, eq 59 is somewhat more complex. By including the restriction that $A < 1$, a mechanical sink term for the areal fraction of ice has been added to a simple continuity equation for the ice concentration. This sink term turns on when $A = 1$ (i.e., no open water left) and under converging conditions removes enough ice area through ridging to prevent further increase in A. Although the sink term does not change the ice mass, it can cause the "thick" ice thickness to increase by allowing h to increase while A does not. This simple sink term is the equivalent of the Thorndike et al. (1975) mechanical redistribution. Hence, within the two-level model the whole ridging process is approximated by specifying that $A < 1$. Note that however this ridging problem is formally treated in this two-level model it does not affect the conservation of ice mass, which is explicitly guaranteed by eq 58. This explicit treatment of the ice mass continuity equation directly is one of the main simplifications of the two-level model over the multi-level treatment.

Treatment of the thermodynamic terms S_A and S_h in eq 58 and 59 varies with investigators, and can make a significant difference in the physics. In ice forecasting applications (e.g. Nikiforov 1957, Doronin 1970), the S_A term is often omitted and A is simply taken as the area covered by ice (as opposed to open water). In longer term seasonal simulations (Hibler 1979, Parkinson and Washington 1979) S_A has been used to cause the thin ice fraction to disappear in proportion to the ice growth rates. Under these formulations (1-A) represents the combined fraction of thin ice and open water.

To couple the ice strength to the ice thickness characteristics the ice strength P* is taken to be a function of compactness and thickness according to

$$P^* = P_o h \exp [-C(1 - A)] \tag{60}$$

where P_o and C are fixed empirical constants and h is in meters. This formulation makes the strength strongly dependent on the amount of thin ice (characterized by the compactness A), while also allowing the ice to strengthen as it becomes thicker.

While directly intuitive, the strength expression in eq 60 can also be qualitatively related to the strength assumptions used in the multi-level thickness approach discussed above. There, under converging conditions, the closure of both thin and thick ice (and also open water) occurs simultaneously. The relative amount of thin ice being deformed, however, is weighted by the area of thick ice. Hence, for small amounts of thin ice, more thick ice is deformed, and thus the ice has a high strength which is dependent on the thick ice characteristics. For a large amount of thin ice, on the other hand, mostly thin ice is deformed, which yields low strength. These features are represented in eq 60 by the exponential dependence on (1 - A), which characterizes the amount of thin ice being ridged, and the proportionality to h, which approximates the strength of thick ice undergoing deformation. The assumption in the h dependence is that the distribution of thick ice is reasonably well described by its mean (h/A). However, while qualitatively correct, this two-level ice thickness scheme does not allow the particular thickness of ice involved in ridging to be determined.

A numerical comparison of thickness-strength coupling

To give some feeling for the role of thickness-strength coupling in the two-level and multi-level models we briefly discuss here the results of simulations of the Arctic Basin ice cover. In order to compare the behavior of the two-level and multi-level models, one-year simulations employing the same forcing of the Arctic Basin ice cover are compared. These simulations consisted of integrating the coupled continuity and momentum balance equations for each model over one seasonal cycle for the Arctic Basin ice cover. While not to seasonal equilibrium, the results are useful for comparing ice strength formulations. Complete details on the numerical framework for these simulations and the forcing fields are described in Hibler (1979, 1980a). Since our main concern is the ice buildup we will not go into the details of the forcing fields (and heat storage in the oceanic boundary layers), which are discussed in the above references. The two main parameter sets of interest for this discussion are P_o ($= 5\times10^3$ N m^{-2}),

C = 20, the strength constant for the two-level case, and H* (=50 m), the ridging specification parameter for the multi-level case (see eq 52). In the two-level case the ice strength is given by eq 60, while in the multi-level case the strength is specified by combining eq 48 with eq 44, 46, 49 and 52. In all cases a uniform initial thickness of 3.3 m was specified everywhere.

Figure 16 shows the December thickness contours for both models. The boundaries employed in the simulation are specified by the solid lines. Also, at the Greenland-Spitsbergen passage an "open boundary" condition (see Hibler 1979) was used, which allowed ice inflow and outflow. As can be seen, both the multi-level and two-level models yield very similar ice thickness buildup, with thicker ice near the archipelago and thinner ice near the pole and off the Alaskan and Siberian coasts. This thickness buildup is due to the ice dynamics, which tends to pile up ice off the archipelago while removing it from other regions. In both models, as this ice gets thicker it gets stronger and tends to prevent further convergence. The main feature illustrated by this figure is, however, the similarity of the thickness contours in the two simulations, despite the differences in ice thickness parameterizations. Both these thickness contours are in good agreement with observations of thickness characteristics in the Arctic Basin, which show a greater buildup along the archipelago, with typical mean thicknesses of about 5-7 m (see, e.g., Wadhams 1981).

It should be noted that one quantitative difficulty with both these simulations is the use of eight-day averaged winds (from May 62 to May 63) in the forcing fields. More recent two-level simulations, with daily time-varying winds of the Arctic ice cover (Hibler and Walsh 1982) and portions of the Antarctic ice cover (Hibler and Ackley 1982, 1983), have yielded higher best fit strength constants, P_o, for the two-level model of 2.75×10^4 N m^{-2}. This value is about five times larger than the best fit P* value use by Hibler (1979) and also used above. The main reason for this increase is that due to the nonlinear wind stress, daily wind fields yield a larger average wind force. As a consequence, a larger ice interaction is needed to yield modification of the ice drift in agreement with observations.

Small scale ramifications of coupling between ice strength and thickness characteristics

As discussed above, the main effect of thickness-strength coupling on the large scale is for the ice to become stronger in regions of convergence, which in turn prevents further convergence. While this same behavior also occurs on smaller scales, there can be a number of fluctuating effects, such as kinematic waves, which are masked on larger scales. Some of these effects depend on the nonlinear ice interaction and the nonlinear coupling between ice strength and thickness characteristics. To yield some insights into these small scale effects Hibler et al. (1983) analyzed some special idealized cases of the two-level model using the same grid as shown in Figure 7. The essential feature of these results is that for a nonlinear model it is possible for ice velocities at a given location to fluctuate in time, even though the wind forcing may be fixed.

Analytical analysis of coupled one-dimensional systems. To demonstrate the overall nature of plastic buildup on a small scale it is useful to analyze an idealized one-dimensional system. As in the momentum-bal-

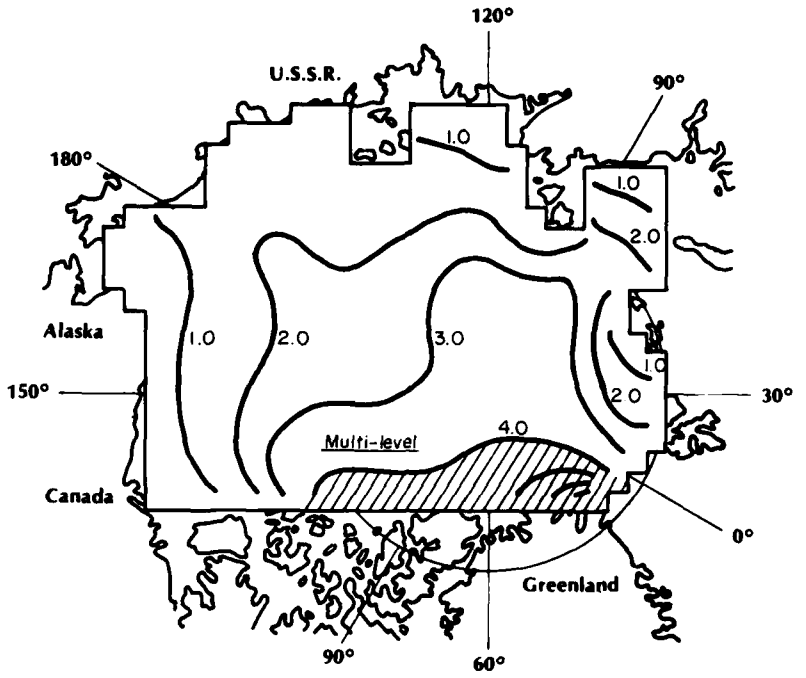

a. Results from a multi-level simulation employing eight thickness levels and an ice strength based on an assumed redistribution process (see eq 44, 46, 48, 49 and 52).

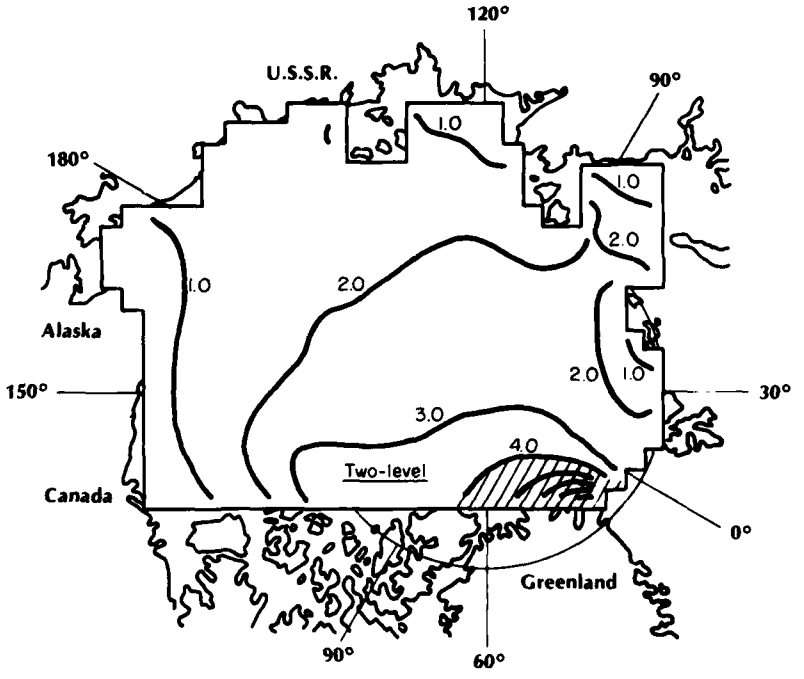

b. Results from a two-thickness level simulation using an empirical ice strength formulation (eq 60).

Figure 16. Simulated 30-day (day 331-360) averaged ice thickness contours in meters for comparative one-year simulations.

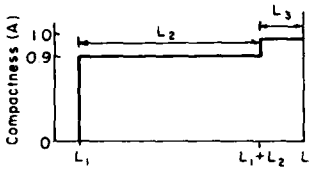

Figure 17. Geometry of idealized one-dimensional compactness conditions.

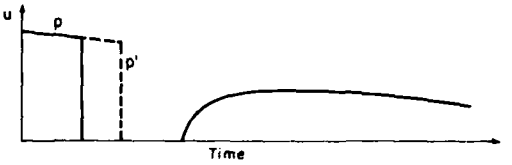

Figure 18. Qualitative plot of velocity versus time for two points in idealized one-dimensional build-up example.

ance-only case (see p. 11-14) consider a one-dimensional system having a linear water drag, rigid plastic interaction, and constant wind field τ from left to right. To simplify analysis the strength P* is taken to depend only on the compactness A. The initial condition consists of a compactness (A) of 0.9. For the coupling of P* to A let us consider P* discontinuously changing at A = 1 as follows:

$$P^*(A) = \begin{cases} -P_1 \text{ if } A < 1 \\ -P \text{ if } A = 1 \end{cases} \tag{61}$$

where $P > P_1$. Because of this discontinuous change the local momentum balance will not be modified by any changes in compactness until the compactness goes to 1. Based on the analysis of the momentum balance only in section 4-c all deformation takes place at a right-hand boundary. Consequently, at some arbitrary time Δt after the initiation of motion we would expect the geometry in Figure 17 to apply. By the earlier momentum balance analysis, for $(P-P_1) < \tau L_3$ all velocities in the L_3 region (compactness of 1) will be zero. Also by the momentum balance analysis the velocities in the L_2 region will be given by

$$U_2 = (\tau L_2 - P_1)/cL_2 \tag{62}$$

so that as L_2 becomes smaller U_2 will slow down somewhat unless $P_1 = 0$. Since with the L_3 region motionless all the deformation is occurring at the L_2,L_3 boundary, it is clear that the L_2,L_3 boundary will propagate outward (to the left) at a speed of $U_2/0.1$. However, note that for L_3 large enough (i.e. $L_3 > (P-P_1)/\tau$) the L_3 region will start moving again with a speed

$$U_3 = (\tau L_3 - (P-P_1))/cL_3. \tag{63}$$

When this occurs the propagation of the ridging front will slow down somewhat to $(U_2-U_3)/0.1$. Also, once all the ice is converted to 100% compactness, the speed will then slowly decrease as the length L_3 decreases due to removal of ice by ridging at the right-hand boundary. Based on these considerations one can construct a qualitative speed versus time of two arbitrary points, say p and p', where p' is located further left than p (Fig. 18).

Obviously, by varying strengths and/or the wind forcing the various slopes, magnitudes and spacing in time of these profiles can be modified. One of the more interesting features of the system is that due to the complexities of the thickness coupling, for appropriate strength differences,

points near the right-hand coast will actually stop for a while and then speed up, even though external forcing is constant. The essential physics here is that because of the discontinuous nature of the ridging front and the nonlinear rheology, points in the L_3 region will not move at all until L_3 becomes large enough to accumulate an adequate wind fetch to overcome the differential of plastic stresses at the boundaries.

Numerical investigation of response characteristics of coupled system. A series of two-dimensional numerical simulations yielded results that generally agree with the one-dimensional analysis. However, there are significant differences associated with the fact that P* does not change discontinuously but is instead a smooth function of A. For the standard case study, the coupled equations were integrated for 18 hours at 15-minute time steps using the grid of Figure 7. The initial conditions consisted of 10% open water together with a mean ice thickness of 0.5 m. To simplify analysis the ice strength is taken to depend only on the compactness, not the ice thickness. As a consequence the ice strength in these particular idealized studies P* is given by

$$P^* = (0.5\ \text{m})\ P_o\ e^{-C(1-A)} \tag{64}$$

To make the test more comparable to the one-dimensional analysis, turning angles and the Coriolis parameter were set equal to zero. A constant wind speed of 9.23 m/s in the positive x direction was used, together with an ice strength constant P_o of 2.0×10^4 N m^{-2}, and a constant C of 30. Other parameters are the same as in Table 1.

The basic characteristics of this idealized numerical simulation are shown in Figure 19, which shows x velocity components versus time for several grid points. These curves were taken from grid points and grid cells centered in the y direction. The general behavior of the velocity-time series is commensurate with the idealized one-dimensional analysis, with the points nearest the coast rapidly decreasing in speed, with a later increase as the region of ridging moves further out. However, there are

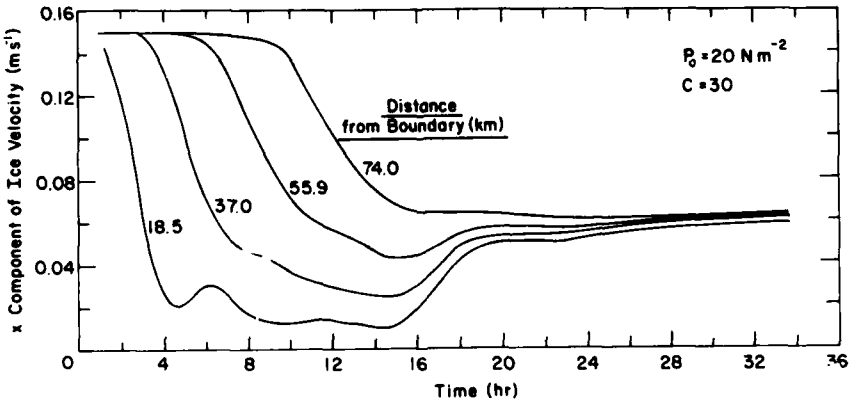

Figure 19. Time series of x component of ice velocity progressively further from right-hand boundary of numerical buildup experiment. The grid points plotted were centered in the y direction and the distances from the right-hand boundary are labeled.

significant differences from the analytic case associated with the fact that the motion near the coast is balanced by a gradient in compactness rather than a discontinuous change. This gradient means a) that the points do not ever totally stop (since some convergence must occur everywhere to allow the gradient to move outward) and b) that the kinematic waves are allowed to propagate upstream (or more precisely down the stress gradient).

These waves arise from the fact that the velocity of ice is balanced in part by the stress gradient, while the stress gradient is maintained by a convergence of the ice velocity field. As a consequence, a perturbation of either one of these quantities can cause a wave to propagate down the stress gradient slope. This wave can naturally develop in the evolution of the system since the initial buildup can be out of equilibrium with regard to kinematic waves (when the dependence of strength on compactness is nonlinear). Such a kinematic wave is apparent in Figure 19 at hour 6 in the velocity time series of the point nearest the coast. Tests at smaller time steps verified that this wave was not a numerical artifact. Closer examinations of this wave show it to slow down somewhat and diffuse as it progresses outward. More detailed investigations of the characteristics of these waves are needed.

THE ROLE OF ICE DYNAMICS IN THE ATMOSPHERE-ICE-OCEAN SYSTEM

General discussion

The fact that ice is moving and deforming rather than static has important ramifications. A feature that has been emphasized a great deal recently is the fact that dynamics creates thin ice and leads in an ice cover (Maykut 1978, Washington et al. 1976). However, in addition to creating leads the dynamics also causes advective effects which can play a pivotal role in the atmospheric and oceanic circulation. In the presence of a free ice edge, for example, advective effects can transfer ice to the marginal regions to be rapidly melted. When viewed from a satellite photo such an ice cover may appear static, since the ice extent does not rapidly change. However, the actual physics maintaining such a "static" extent can be complex and largely dependent upon processes occurring at the ice margin.

Advection also causes net imbalances of ice growth by transferring ice from regions of high growth to regions of greater melt. Since most of the salt is taken out of the ice when it freezes, the high growth regions will be regions of high salt flux into the ocean, whereas the high melt regions will be areas of fresh water input. These features can significantly alter the oceanic circulation and vertical convection. With regard to the atmosphere, regions of high growth are regions of high heat exchange with the atmosphere due to the latent heat of freezing of the ice cover. A third, rather indirect way ice dynamics can affect the atmosphere-ocean heat exchanges has recently been noted by Hibler and Ackley (1982). They carried out several simulations invoking an ice feedback mechanism similar to that used in many simple climate models, whereby the presence of ice caused the lower atmosphere to be cooled. With this feedback mechanism, simulations without dynamics produced very unrealistic summer ice margins, whereas simulations with dynamics produced a realistic delay. Basically, the dynamics affords a mechanism for "turning off" the feedback link, which is not possible in the purely static thermodynamic models.

Finally, in addition to modifying the thermal and salinity fluxes at the air/ocean interface, sea ice can substantially modify the momentum transfer by wind to the ocean. Specifically, if we consider the ice-ocean system to be coupled, then the momentum transfer into the ocean is given by the wind stress less the force due to ice interaction. As discussed earlier, due to the highly nonlinear ice interaction the ice stress terms can be very complex.

To illustrate the relative importance of some of these features, results from two series of simulations of the Weddell Sea pack ice are discussed in the following subsections. The first subsection describes simulations of the Weddell Sea pack ice, while the second subsection examines the salient characteristics of an ice-covered Arctic Ocean model. A more complete description of these simulations is given elsewhere (Hibler and Ackley 1983, Hibler and Bryan 1984).

Results from a Weddell Sea pack ice model

Model description. The model essentially consists of a momentum balance employing a plastic rheology coupled to the two-thickness evolution equations for the ice thickness and compactness discussed earlier (eq 58-60). These equations also include ice growth and decay due to surface heat budget considerations and heat storage in a motionless fixed-depth oceanic boundary layer. For the ice strength (see eq 60) we take $P_o = 2.75 \times 10^4$ N m^{-2} and $C = 20$. This P_o value is about five times larger than the P_o value used by Hibler (1979). This increase was necessitated by the fact that daily wind fields were used here as opposed to the eight-day average wind fields used by Hibler (1979).

Following formulations developed by Hibler (1979), the thermodynamic terms in the continuity equations (58 and 59) are given by

$$S_h = f(h/A)A + (1 - A)f(0) \tag{65}$$

$$S_A = \begin{cases} (f(0)/h_o)(1 - A) & \text{if } f(0) > 0 \\ 0 & \text{if } f(0) < 0 \end{cases} + \begin{cases} 0 & \text{if } S_h > 0 \\ (A/2h)S_h & \text{if } S_h < 0 \end{cases} \tag{66}$$

with $f(h)$ the growth rate of ice of thickness h, and h_o a fixed demarcation thickness between thin and thick ice.

The S_h term specifies the net ice growth or melt. Within the two-level approximation, S_h is given by the sum of the ice grown on open water plus the additional growth over the portion of the cell covered by thick ice. To approximate the growth and decay rate of this thick ice, its mean growth rate is estimated to be that of ice of constant thickness h/A. For melting conditions the same sum over open water and thick ice is used. A critical assumption here is that the heat absorbed by open water will horizontally mix and melt additional ice until the mixed layer returns to freezing.

The S_A term characterizes the way in which growth and decay change the relative areal extents of thin and thick ice. The basic physical notion embodied by this term is that the areal fraction of thin ice will decrease rapidly under freezing conditions, and increase slowly under melting conditions. To parameterize the freezing effect simply, the fraction of open water (1 - A) is allowed to decay exponentially with a time constant of $h_o/f(0)$, which gives the first term in eq 66. The constant h_o is chosen to be small compared to mean ice thicknesses but large enough so that heat fluxes through h_o-thick ice are substantially less than through open water. In the Arctic simulations performed by Hibler (1979) $h_o = 0.5$ m is used. However, for these Antarctic simulations h_o is set equal to 1.0. This larger value is based on field observations reported in Ackley et al. (1980) and Gow et al. (1982), which suggest that frazil ice formation may well prolong ice production in open water regions. Other than h_o and P_o, the numerical parameters used in the simulation are identical to those used by Hibler (1979) and Hibler and Walsh (1982).

The second term in eq 66 accounts for melting. Its magnitude is derived by assuming that the thick ice is uniformly distributed between 0 and 2 h/A in thickness, and all melts at the same rate. Therefore, over a time Δt the ice of thickness less than $S_h \Delta t$ will melt and form open water. By the assumption of uniform distribution this ice covers a fraction of area equal to $S_h \Delta t\, A/2h$, which for Δt small yields the second term in the equation for S_A.

The vertical growth rates (f(h)) are estimated by employing Semtner's (1976) sea ice thermodynamic model in conjunction with a surface heat budget calculation similar to that of Parkinson and Washington (1979) and Manabe et al. (1979). The basic surface energy budget calculation (for details see Hibler, 1980a, Appendix B) includes incoming shortwave and longwave radiation and sensible and latent heat fluxes, and provides for the determination of the surface temperature of the ice by numerical iteration.

Following Manabe et al. (1979), the effects of snow cover are approximated by allowing the ice surface albedo to be that of snow when the calculated surface temperature is below freezing, and that of snow-free ice when the surface temperature of the ice is at the melting point. The model also includes a motionless oceanic mixed layer of fixed depth (30 m) and assumes a constant oceanic heat flux of 2 W/m^2. In the two-level simulation, when open water is absorbing heat all of the absorbed heat is used to further melt the ice. If there is no ice the absorbed heat raises the temperature of the mixed layer. Under growth conditions, no ice is allowed to form until the mixed layer reaches the freezing temperature of seawater.

Input fields. Input fields to drive the model consist of average daily surface atmospheric air temperatures, mixing ratios, and surface pressure taken from the 1979 Australian analysis. Preliminary simulations with these analyzed atmospheric temperature fields yielded unrealistically small ice concentrations in summer. Comparison of analyzed surface temperature with buoy observations indicated that the main problem was the excessively high temperatures in the late summer and fall (February-April) in the Australian surface analysis, which did not include these buoy observations. Two procedures were examined to construct a more realistic surface analysis. In a crude reanalysis method, hereafter referred to as the standard case, air temperatures and mixing ratios were not allowed to rise above

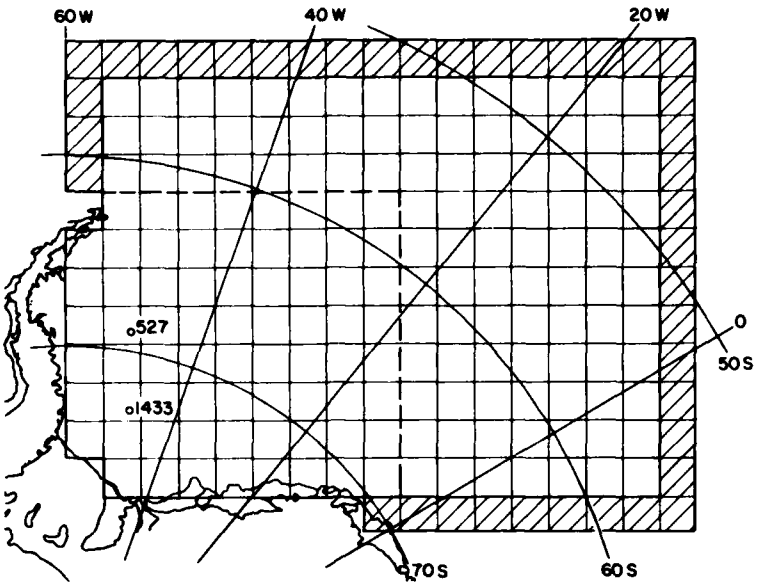

Figure 20. Grid used for numerical simulations of the Weddell Sea pack ice. The dashed line encloses the area where the temperature and humidity fields were reanalyzed. The hatched grid cells represent open boundaries which allow inflow or outflow of ice, and are taken to have 0 strength for ice dynamics calculations (see Hibler, 1979, for a more complete discussion of these open boundaries). The open circles denote the 1 January 1979 positions of two drifting buoys.

271.2 K and 0.25 g kg^{-1} in the region designated by the square box in Figure 20 in all months except January. Slightly different regions were experimented with but had little effect on the results. For the more fully coupled case, the air temperature and the humidity were related to the presence of ice by specifying maxima of 271.2 K and 0.25 g kg^{-1} for the temperature and mixing ratios if the ice cover concentration was greater than 0.50 (or in the case of the thermodynamics-only model if the ice thickness was less than 25 cm). It is notable that such a "feedback" mechanism is consistent with field observations (S.F. Ackley, private communication) near the ice edge, suggesting that the air temperature undergoes an abrupt change as the ice edge is crossed. Also, measurements of atmospheric boundary layer modification (Andreas et al. 1979) support the assertion of a feedback between atmospheric temperature and ice extent.

For the calculation of geostrophic ocean current fields, mean dynamic topography values reported by Gordon et al. (1978) were used. In the radiation calculations, parameterizations similar to those employed by Parkinson and Washington (1979) were used. Specifically, daily global solar radiation under cloudless skies was obtained by integrating an empirical equation by Zillmann (1972) over solar zenith angles for any particular day. [Zenith angles at half-hour intervals for this purpose were obtained from a numerical solution of Kepler's equation (Holloway, personal communication).] Incoming longwave radiation was obtained using Idso and Jackson's (1969) formula for clear skies. For cloud cover, a constant value of

0.85 was assumed at all points. This value is commensurate with maximum estimates by Van Loon (1972).

Simulation results. Using the modified input fields and feedback parameterization discussed above, two-year simulations were carried out using a) the full coupled model and, for comparison, b) only the thermodynamic portion of the model, and c) a version including leads but no advection. This latter case was obtained by using the continuity equations

$$\frac{\partial A}{\partial t} = (\nabla \cdot \underline{u})A + S_a \tag{67}$$

$$\frac{\partial h}{\partial t} = S_h = f(h/A)A + (1-A)f(0). \tag{68}$$

To generate the leads, the ice velocity field from the second year of the standard fully coupled simulation was used. Note that no ridging is considered in this case. Basically, with this "leads-only" case deformation only enters by affecting A, which in turn modifies the average growth rate S_h over a given region. In all cases the initial condition consisted of 2 m of ice everywhere. Comparison of these results gives some insight into the role of ice dynamics on the ice edge fluctuations and the effects of ice-atmosphere feedback on the seasonal cycle of ice.

Some selected ice extent results from these simulations are illustrated in Figure 21, which shows plots of the ice concentration for the full model and thin ice contours for the thermodynamics-only case employing the standard forcing. The observations are based on Fleet Weather ice charts (prepared by the Navy-NOAA Joint Ice Center, Suitland, Md.) and denote 50% ice concentration limits. In most cases this 50% limit is effectively at the ice edge estimated in the Fleet Weather charts. In this figure two different days were chosen to represent salient features of both the simulated and observed ice extents. Day 18 (18 January) represents a period close to the end of the rapid decay and shows a characteristic geometric tongue of ice often seen at this time of year. Day 298 (25 October), on the other hand, represents a typical maximum extent at a time just prior to the beginning of the rapid decay phase.

As can be seen from Figure 21, on day 18 the full model reproduces the tongue effect and ice extent much better than the thermodynamics-only case. Analysis of the ice velocity field (see the next section) shows that this tongue is largely due to northward and eastward advection of ice by the ice velocity field. (The tongue is, however, a bit too far south, partially due to insufficient northward ice transport as discussed in the next section.) In the thermodynamics-only case the structure of the ice edge is totally incorrect and there is too much ice.

On day 298 the results are, however, quite similar, with both the full model and the thermodynamic case showing extents slightly less than observed. This in turn indicates that the expansion to maximum is largely thermodynamic in nature and controlled (in both simulations) by the temperature field.

The effect of dynamics on the seasonal variation is illustrated more graphically in Figure 22, which shows the observed time series of the total

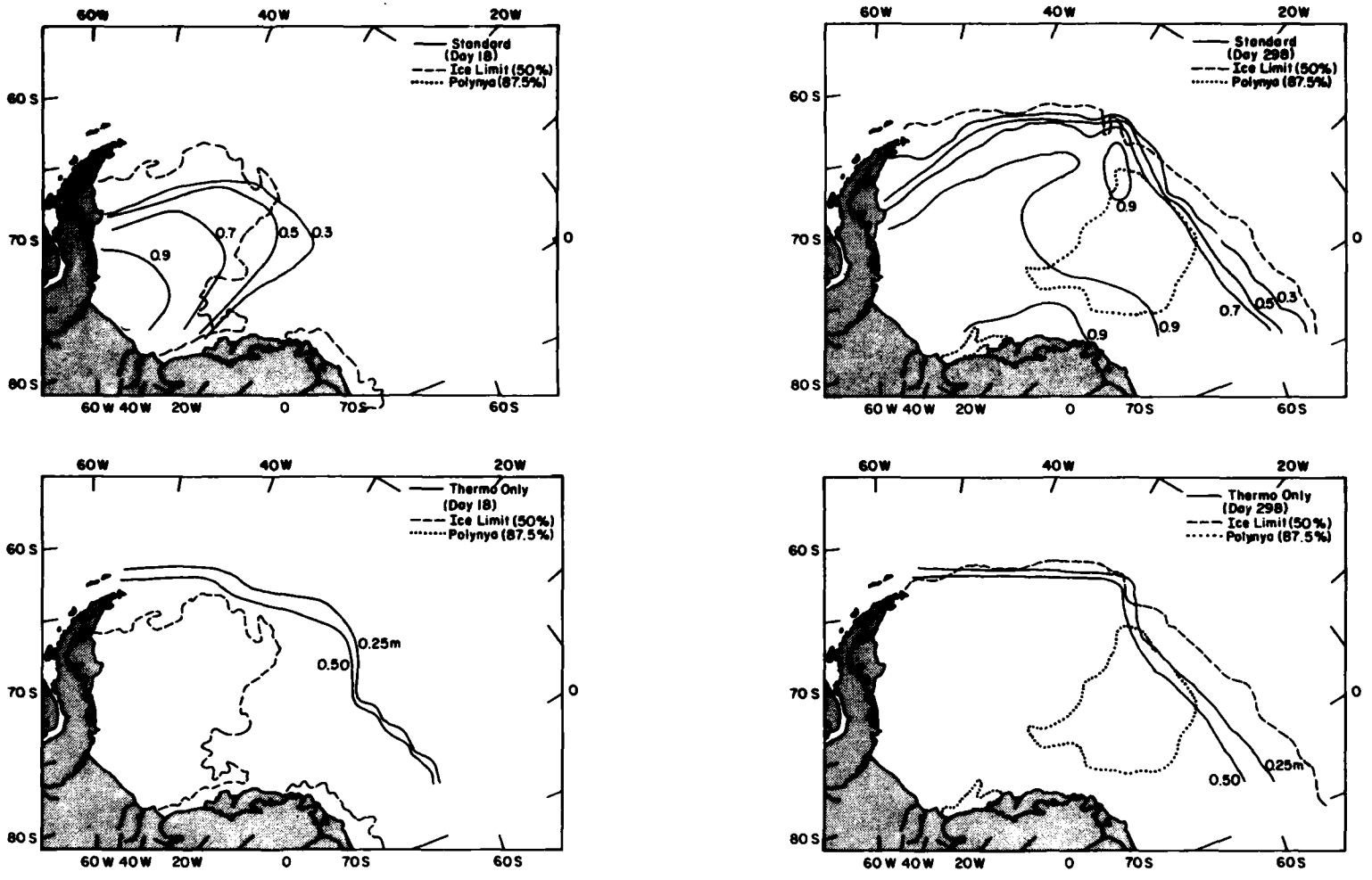

Figure 21. Simulated and observed ice concentrations and extent for the full dynamic thermodynamic model (standard) and for the thermodynamics-only case (thermo only). The dashed line denotes the observed limit of ice having a concentration of at least 50%. The dotted line shows interior polynyas having concentrations less than 87.5%.

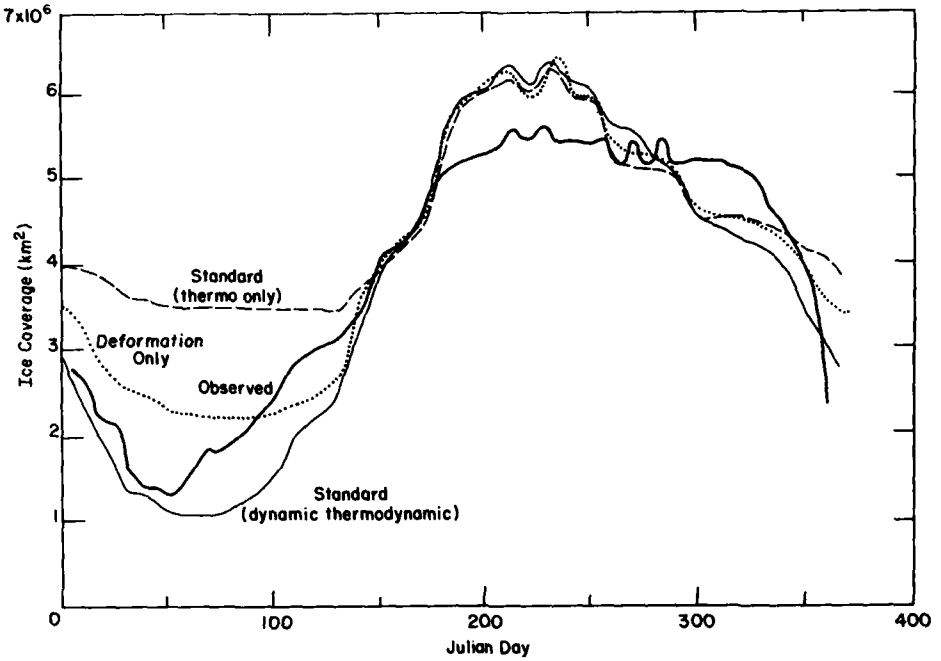

a. Results using the reanalyzed temperature and humidity fields.

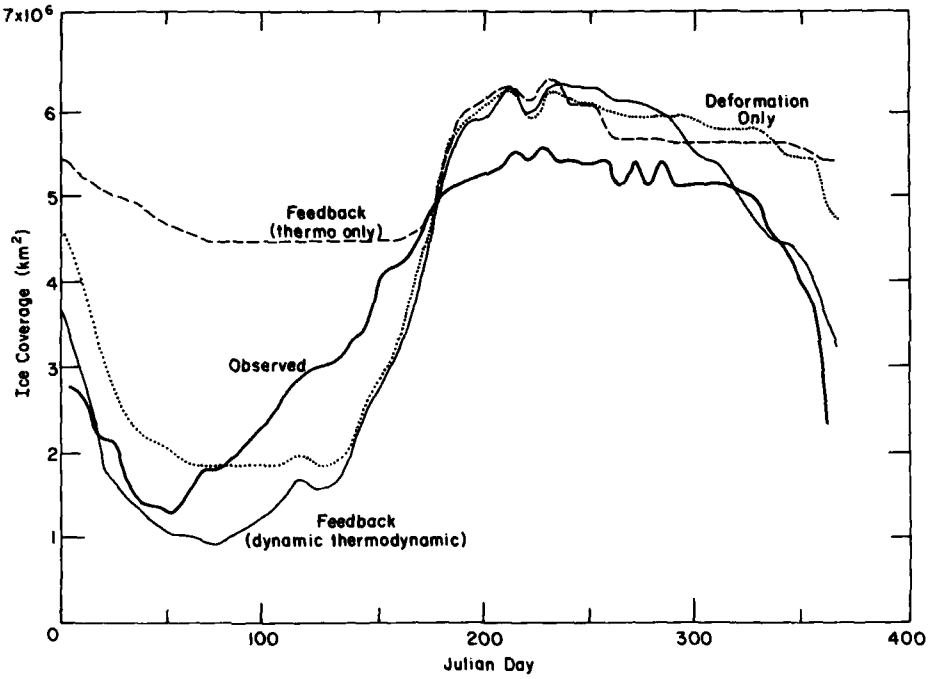

b. Results using the feedback parameterization between the atmosphere and the ice discussed in the text.

Figure 22. Time series of total area covered by ice within the simulation region.

grid area covered by ice with concentrations greater than 15%. This figure includes simulations using both the "feedback" (part b) forcing and the "standard" forcing (part a). Also shown in this figure are the time series of the thermodynamics-only case and of the "leads-only" simulation. In the thermodynamics-only case the area given is for ice of non-zero thickness. As can be seen, the coupled model, with the dynamics included, gives a bigger seasonal swing of extent and a more rapid decay of the ice cover. Both these effects are primarily due to the large amount of deformation and advection caused by the dynamics, which in turn creates open water. As the shortwave radiation terms increase during spring and summer this open water absorbs large amounts of heat and causes a rapid decay of the ice cover. However, a difficulty with the standard case (and the thermodynamics-only case) is a lack of persistence of the ice cover in the spring (day 250 on).

As can be seen, the full model reproduces a realistic seasonal variation and geographical extent. This feature is substantially improved in the feedback case, which produces the persistence in the ice extent in the spring (day 250 on) that is in slightly better agreement with observation than the standard case discussed above, without significantly modifying the rapid decay seen in the summer (December-January) period. Although not shown, the feedback also produces a realistic ice tongue similar to the standard case discussed previously. The thermodynamics-only case, on the other hand, effectively produces a constant ice edge with very little seasonal cycle.

With respect to the simulation including leads, its behavior is similar to the thermodynamics-only case except that it has a bigger seasonal swing. However, the inclusion of leads alone without advection is not adequate to give a realistic seasonal swing. Also, examination of the geographical contours of the leads-only case shows them to be very similar to the thermodynamics-only case, and especially unrealistic in summer. Analysis of the results shows that in the full model the reduced extent is partially due to winds near the ice edge -- winds which tend to shift the whole ice edge eastward and thus reduce the extent.

A notable feature of these simulations is that for the forcing employed here it is not necessary to increase the oceanic heat flux above typical Arctic values to obtain a realistic seasonal cycle when realistic dynamics are included. This is in contrast to calculations based primarily on thermodynamic considerations by previous authors, which have suggested the need for a larger oceanic heat flux to explain the ice decay.

While there are differences in extent, a much more major difference between the full model and the deformation-only and thermodynamics-only models is in the net seasonal ice growth. To examine these characteristics the fully coupled feedback simulation was extended to a third year, and the net annual ice growth calculated. Figure 23 shows the contours of this net ice growth over an annual cycle. In both the leads-only and thermodynamics-only cases the net ice growth is very small, since in seasonal equilibrium all ice growth is balanced by melt. However, with advection included there are drastic changes, with much of the ice growth taking place in southern parts of the grid and ice melt occurring farther north near the Equator. Off the Filchner Ice Shelf the ice growth exceeds 3 m. High growth in this region is known to be a major factor in bottom water formation, and the numbers obtained from the simulation are commensurate with

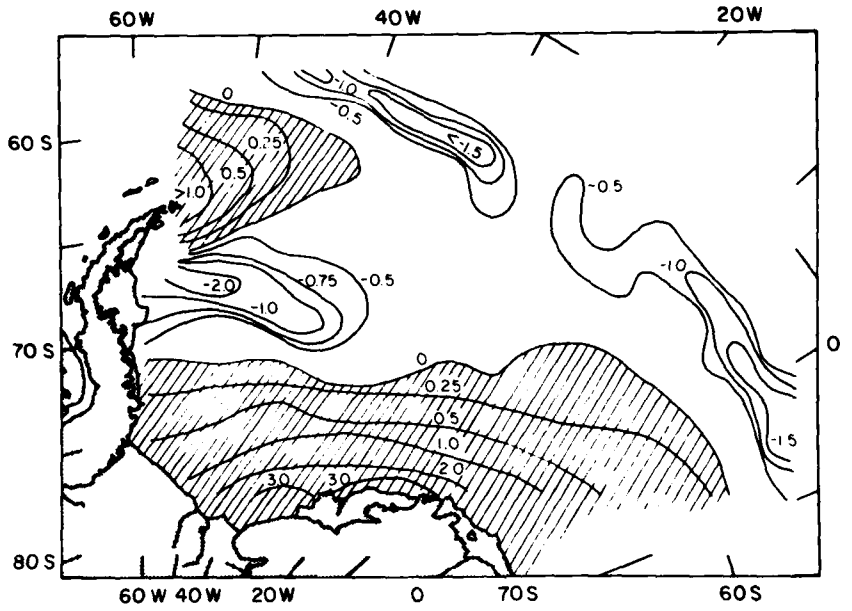

Figure 23. Contours (in meters) of the net annual ice growth over an annual cycle for the fully coupled dynamic thermodynamic model. The contours were compiled from the third year of the feedback simulation.

maximum estimates in the literature (see, e.g., Ackley 1980) based on oceanographic considerations. Also, the fact that ice melting takes place at different locations than growth means that large amounts of fresh water can effectively be transported to different regions of the Weddell Sea, a factor of some importance in the pycnocline structure there. Note also that much of the melt is highly concentrated at the ice edge, illustrating a conveyor-belt-like effect whereby ice is transported to the edge to be melted.

Ice edge characteristics of an ice-covered Arctic Ocean model

In the simulations of Antarctic sea ice discussed above, realistic ice edge results were obtained with the ocean parameterized by only a motionless fixed-depth mixed layer. In the Greenland/Norwegian Seas, however, such an approximation (see, e.g., Hibler and Walsh 1982) yields unrealistically large ice extents. This is not surprising in that large scale oceanic circulation effects would be expected to be particularly pronounced in the Greenland and Norwegian Seas due to warm northward currents encountering rapidly cooling atmospheric conditions and southward-advancing sea ice. In order to examine the dominant effects of the full three-dimensional ocean circulation on the simulated ice margin and to examine ice-ocean coupling effects, Hibler and Bryan (1984) constructed a diagnostic ice-ocean model and used it to carry out a series of seasonal simulations of the Arctic, Greenland and Norwegian Seas. The term "diagnostic" refers to the fact that temperature and salinity fields are largely specified by observed data by a relaxation method rather than fully simulated. However, as discussed below this relaxation is done in a relatively weak manner so that seasonal and month-to-month variations in the temperature and salinity

due to ice-ocean coupling effects will be simulated by the model. Some of the salient results of these simulations are briefly described here.

In this study an existing dynamic-thermodynamic sea-ice model (Hibler 1979, 1980) was coupled with a multi-level baroclinic ocean model (Bryan 1969). The sea-ice model (essentially equivalent to the Weddell Sea pack ice model described above) supplied heat flux, salt flux, and momentum exchange boundary conditions for the top of the ocean. The ocean model, in turn, supplied current and heat exchange information to the ice model. Since the concern here was to examine the effect of ocean circulation on sea ice, observed oceanic temperature and salinity data (Levitus 1982) were used to weakly force the ocean model so that its equilibrium time scale is similar to that of the ice model (3 to 5 years). This forcing is done by adding additional source terms to the heat and salt conservation equations of the form $R\ [T_o - T]$ and $R\ [S_o - S]$. Here R is a relaxation constant taken to be 0.333 yr^{-1}, and T_o and S_o are the mean annual observed temperature and salinity fields. This "diagnostic" method allows the ocean model to be forced to available climatological ocean data, while at the same time allowing considerable adjustment in the upper ocean due to the effects of ice/ocean interaction. In addition, the barotropic mode of the ocean is fully simulated so that temporally varying currents due to surface stress fluctuations are part of the model predictions. The basic idea here is to specify rather than model the ocean circulation over climatic time scales while modeling the shorter term fluctuations.

The most noticeable effect of the modeled ocean circulation is to greatly improve the ice margin simulation, as shown in Figure 24a. This improved ice margin is due to the large oceanic heat flux from the deeper ocean into the upper mixed layer in this region. The heat flux occurs primarily in winter and analysis shows that much of the enhancement is due to deep convection which brings up warm water and prevents ice formation in early winter. This convection explains the absence of ice in the full model simulation far from the ice margin.

Near the ice margin a similar physics applies, but the precise location of the ice edge becomes more sensitive to the surface salt balance and to lateral effects in the oceanic circulation. The sensitivity simulations shown in Figure 24b, for example, indicate that the freshwater flux from melting at the advancing ice edge tends to seal off the ice margin to upward oceanic heat flux and allows a farther advance than would otherwise occur. A sensitivity simulation without lateral motion in the ocean (Fig. 24b) also tends to produce a more excessive edge at the end of one year, since the lateral transport of heat to both the deep and upper layers is missing. This latter result demonstrates the difficulty of simulating the seasonal cycle of sea ice using only a one-dimensional mixed layer model.

An additional interesting feature of this coupled ice-ocean model is the modification by the ice interaction of the wind stress transferred into the ocean. This effect is particularly pronounced on long time scales since large fluctuations in wind stress tend to average out. Analysis of the nine-month average wind and ice stresses at buoy locations in the Arctic Basin, for example, shows forces due to the ice interaction to typically be in opposition to the wind stress and to have similar magnitudes. However, in some cases the ice stress can combine with the wind stress or be at right angles to the ice drift due to the configuration of the land

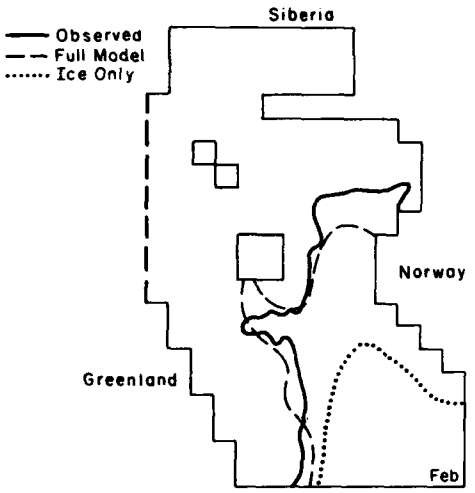

a. February 50% concentration limits from the full coupled ice/ocean model and for the ice-only model, which includes a fixed-depth mixed layer. The observed limit is taken from Fleet Weather (Suitland, Md., U.S. Navy) charts for the end of February.

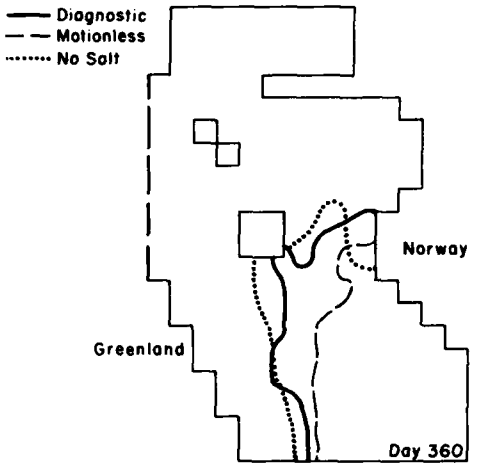

b. Simulated 0.05 m thickness contours for day 360 for the full model, a "motionless" ocean model, and a coupled ice/ocean model with no salt fluxes due to ice freezing and melting. The "motionless" model and the no-salt simulations were run for only 1 year and were initialized to ice thickness and ocean fields at the end of the fourth year of the full diagnostic model simulation.

Figure 24. Comparisons of simulations of ice concentration and ice thickness (from Hibler and Bryan 1984).

boundaries and the ice edge. In addition, near certain boundaries the ice interaction was found to introduce not only magnitude changes but also sign changes in the curl of the stress transmitted into the ocean. Such effects should be particularly relevant to longer term prognostic ocean simulations, and emphasize the need for better understanding of the nature of ice interaction.

CONCLUDING REMARKS

Sea ice dynamics deals with the way momentum and energy are distributed at the air/ice/ocean interface. As such, it plays a pivotal role in describing air-sea interaction in polar regions. Because these sources of energy and momentum are often external to the ice, understanding sea ice dynamics entails studying the coupled air-sea-ice system. This review has shown that sea ice dynamics can cause substantial modification to the air-

sea momentum, heat, and salt exchanges. Examination of the consequences of these modifications for the atmosphere and ocean is just beginning. From the work reviewed here, however, it is evident that to understand these modifications the nonlinear interaction of sea ice must be considered. Further studies are needed to improve our understanding of the interaction, especially near the ice margin.

LITERATURE CITED

Ackley, S.F. (1980) Mass balance aspects of the Weddell Sea pack ice. Journal of Glaciology, 24: 391-405.

Ackley, S.F., A.J. Gow, K.R. Buck and K.M. Golden (1980) Sea ice studies in the Weddell Sea aboard USCGC Polar Sea. Antarctic Journal of the United States, 15(5): 84-86.

Andreas, E.L., C.A. Paulson, R.M. Williams, R.W. Lindsay and J.A. Businger (1979) The turbulent heat flux from Arctic leads. Boundary Layer Meteorology, 17: 57-91.

Brown, R.A. (1980) Planetary boundary layer modeling for AIDJEX. In Sea Ice Processes and Models (R.S. Pritchard, Ed.). University of Washington Press, pp. 387-401.

Bryan, K. (1969) A numerical method for the study of the circulation of the world oceans. Journal of Computational Physics, 4: 347-376.

Campbell, W.J. (1965) The wind-driven circulation of ice and water in a polar ocean. Journal of Geophysical Research, 70: 3279-3301.

Colony, R. and D.A. Rothrock (1980) A perspective of the time-dependent response of the AIDJEX model. In Sea Ice Processes and Models (R.S. Pritchard, Ed.). University of Washington Press, pp. 124-133.

Coon, M.D. (1974) Mechanical behavior of compacted arctic ice floes. Journal of Petroleum Technology, 26: 466-470.

Doronin, Yu. P. (1970) On a method of calculating the compactness and drift of ice floes. Trudy Arkticheskii i Antarkticheskii, Nauchno-Issledovatelski Institut, 291: 5-17. (English translation, AIDJEX Bulletin, 3: 22-39, 1971.)

Egorov, K.L. (1970) Theory of drift of ice floes in a horizontally heterogeneous wind field. Problemy Arkticheskii i Antarkticheskii, 34: 71-78. (English translation, AIDJEX Bulletin, 6: 37-45, 1971.)

Glen, J.W. (1970) Thoughts on a viscous model for sea ice. AIDJEX Bulletin, 2: 18-27.

Gordon, A., E. Molinelli and T. Baker (1978) Large scale relative dynamic topography of the southern ocean. Journal of Geophysical Research, 83: 3023-3032.

Gow, A.J., S.F. Ackley, W.F. Weeks and J. Govoni (1982) Physical and structural characteristics of Antarctic sea ice. Annals of Glaciology, 3: 113-117.

Hibler, W.D. III (1974) Differential sea ice drift. II: Comparison of mesoscale strain measurements to linear drift theory predictions. Journal of Glaciology, 13: 457-471.

Hibler, W.D. III (1977) A viscous sea ice law as a stochastic average of plasticity. Journal of Geophysical Research, 82: 3932-3938.

Hibler, W.D. III (1979) A dynamic thermodynamic sea ice model. Journal of Physical Oceanography, 9: 815-846.

Hibler, W.D. III (1980a) Modeling a variable thickness sea ice cover. Monthly Weather Review, 108: 1943-1973.

Hibler, W.D. III (1980b) Documentation for a two-level dynamic thermodynamic sea ice model. USA Cold Regions Research and Engineering Laboratory, Special Report 80-8.

Hibler, W.D. III, S.F. Ackley, W.K. Crowder, H.W. McKim and D.M. Anderson (1974a) Analysis of shear zone ice deformation in the Beaufort Sea using satellite imagery. In The Coast and Shelf of the Beaufort Sea (J.C. Reed and J.E. Sater, Ed.). Arctic Institute of North America, pp. 285-296.

Hibler, W.D. III, S.J. Mock and W.B. Tucker (1974b) Classification and variation of sea ice ridging in the western Arctic Basin. Journal of Geophysical Research, 79: 2735-2743.

Hibler, W.D. III and W.B. Tucker (1979) Some results from a linear viscous model of the Arctic ice cover. Journal of Glaciology, 22: 293-304.

Hibler, W.D. III, I. Udin and A. Ullerstig (1981) On modeling mesoscale ice dynamics using a viscous plastic constitutive law. In Proceedings of the Sixth International Conference on Port and Ocean Engineering Under Arctic Conditions, Quebec, pp. 1317-1328.

Hibler, W.D. III and S.F. Ackley (1982) On modeling the Weddell Sea pack ice. Annals of Glaciology, 3: 125-130.

Hibler, W.D. III and J.E. Walsh (1982) On modeling seasonal and interannual fluctuations of Arctic sea ice. Journal of Physical Oceanography, 12: 1514-1523.

Hibler, W.D. III and S.F. Ackley (1983) Numerical simulation of the Weddell Sea pack ice. Journal of Geophysical Research, 33: 2373-2887.

Hibler, W.D. III, I. Udin and A. Ullerstig (1983) On forecasting mesoscale ice dynamics and buildup. Annals of Glaciology, 4: 110-115.

Hibler, W.D. III and K. Bryan (1984) Ocean circulation: Its effects on seasonal sea-ice simulations. Science, 224: 489-492.

Hunkins, K. (1975) The oceanic boundary layer and stress beneath a drifting ice floe. Journal of Geophysical Research, 80: 3425-3433.

Idso, S. and R.D. Jackson (1969) Thermal radiation from the atmosphere. Journal of Geophysical Research, 74: 5397-5403.

Kovacs, A. (1972) On pressured sea ice. In Sea Ice: Proceedings of an International Conference. Reykjavik: National Research Council, Iceland. pp. 276-295.

Kovacs, A. and M. Mellor (1974) Sea ice morphology and ice as a geologic agent in the southern Beaufort Sea. In The Coast and Shelf of the Beaufort Sea (J.L. Reed and J.E. Sater, Ed.). Arctic Institute of North America, pp. 113-161.

Laikhtman, D.L. (1964) Physics of the boundary layer of the atmosphere. Translated by U.S. Department of Commerce, Washington, D.C., 200 pp.

Leavitt, E. (1980) Surface-based air stress measurements made during AIDJEX. In Sea Ice Processes and Models (R.S. Pritchard, Ed.). University of Washington Press, pp. 419-429.

Lepparanta, M. (1980) On the drift and deformation of sea ice fields in the Bothnian Bay. Winter Navigation Research Board, Helsinki, Finland, Research Report No. 29.

Levitus, S. (1982) Climatological atlas of the world ocean. NOAA Professional Paper 13, 173 pp.

Malvern, L.E. (1969) Introduction to the Mechanics of a Continuous Media. Englewood Cliffs, New Jersey: Prentice Hall.

Manabe, J., K. Bryan and M.J. Spelman (1979) A global ocean-atmosphere climate model with seasonal variation for future studies of climate sensitivity. Dynamics of the Atmosphere and Ocean, 3: 393-426.

Maykut, S.A. (1978) Energy exchange over young sea ice in the central Arctic. Journal of Geophysical Research, 83: 3646-3658.

McPhee, M.G. (1979) The effect of the oceanic boundary layer on the mean drift of pack ice: Application of a simple model. Journal of Physical Oceanography, 9: 388-400.

McPhee, M.G. (1980) An analysis of pack ice drift in summer. In Sea Ice Processes and Models (R.S. Pritchard, Ed.). University of Washington Press, pp. 62-75.

McPhee, M.G. (1982) Sea ice drag laws and simple boundary layer concepts, including application to rapid melting. USA Cold Regions Research and Engineering Laboratory, CRREL Report 82-4.

Nikiforov, Y.G. (1957) A change in the concentration of the ice cover in connection with its dynamics. Problemy Arktiki, 2: 59-71. (Translated by American Meteorological Society.)

Nye, J.F. (1973) Is there any physical basis for assuming linear viscous behavior for sea ice. AIDJEX Bulletin, 21: 18-19.

Omstedt, A. and J. Sahlberg (1977) Some results from a joint Swedish-Finnish sea ice experiment, March 1977. Winter Navigation Research Board, Norrkoping, Sweden, Research Report No. 26.

Parkinson, C.L. and W.M. Washington (1979) A large-scale numerical model of sea ice. Journal of Geophysical Research, 84: 311-337.

Parmerter, R.R. and M.D. Coon (1972) Model of pressure ridge formation in sea ice. Journal of Geophysical Research, 77: 6565-6575.

Pritchard, R.S. (1975) An elastic-plastic constitutive law for sea ice. Journal of Applied Mechanics, 43E: 379-384.

Pritchard, R.S., M.D. Coon and M.G. McPhee (1977: Simulation of sea ice dynamics during AIDJEX. Journal of Pressure Vessel Technology, 99J: 491-497.

Roed, L.P. and J.J. O'Brien (1981) Geostrophic adjustment in highly dispersive media: An application to the marginal ice zone. Journal of Geophysical and Astrophysical Fluid Dynamics, 18: 263-278.

Rothrock, D.A. (1975a) The mechanical behavior of pack ice. Annual Reviews of Earth and Planetary Science, 3: 317-342.

Rothrock, D.A. (1975b) The energetics of the plastic deformation of pack ice by ridging. Journal of Geophysical Research, 80: 4514-4519.

Semtner, A.J. Jr. (1976) A model for the thermodynamic growth of sea ice in numerical investigations of climate. Journal of Physical Oceanography, 6: 379-389.

Sodhi, D.S. and W.D. Hibler III (1980) Nonsteady ice drift in the Strait of Belle Isle. In Sea Ice Processes and Models (R.S. Pritchard, Ed.). University of Washington Press, pp. 177-186.

Thorndike, A.S., D.A. Rothrock, G.A. Maykut and R. Colony (1975) The thickness distribution of sea ice. Journal of Geophysical Research, 80: 4501-4513.

Thorndike, A.S. and R. Colony (1982) Sea ice motion in response to geostrophic winds. Journal of Geophysical Research, 87: 5845-5852.

Tucker, W.B. III and W.D. Hibler III (1981) Preliminary results of ice modeling in the East Greenland area. In Proceedings of the Sixth International Conference on Port and Ocean Engineering Under Arctic Conditions, Quebec, pp. 867-878.

Tucker, W.B. III and J.W. Govoni (1981) Morphological investigations of first-year sea ice pressure ridge sails. Cold Regions Science and Technology, 5: 1-12.

Tucker, W.B. III, W.F. Weeks and M. Frank (1979) Sea ice ridging over the Alaskan continental shelf. Journal of Geophysical Research, 84: 4885-4897.

Van Loon, H. (1972) Cloudiness and precipitation in the Southern Hemisphere. In Meteorology of the Southern Hemisphere (C.W. Newton, Ed.). Meteorological Monographs, 13: 101-111.

Wadhams, P. (1981) Sea ice topography of the Arctic Ocean in the region 70°W to 25°E. Philosophical Transactions of the Royal Society, London, A302: 1464-1504.

Washington, W.M., A.J. Semtner, C. Parkinson and L. Morrison (1976) On the development of a seasonal change sea-ice model. Journal of Physical Oceanography, 6: 679-685.

Weeks, W.F., A. Kovacs and W.D. Hibler III (1971) Pressure ridge characteristics in the arctic coastal environment. In Proceedings of the FirstInternational Conference on Port and Ocean Engineering Under Arctic Conditions. Trondheim: Technical University of Norway, Vol. 1, pp. 152-193.

Zillmann, J.W. (1972) Solar radiation and air-sea interaction south of Australia. In Antarctic Oceanology II: The Australian-New Zealand Sector (D.E. Haynes, Ed.). AGU Antarctic Research Series, 19, pp. 11-40.

Zubov, N.N. (1943) Arctic Ice. 491 pp. (Translation: National Technical Information Service (AD426972).)

A facsimile catalog card in Library of Congress MARC format is reproduced below.

Hibler, William D. III
Ice dynamics / by William D. Hibler III. Hanover, N.H.: Cold Regions Research and Engineering Laboratory; Springfield, Va.: available from National Technical Information Service, 1984.
v, 58 p., illus.; 28 cm. (Monograph 84-3.)
Bibliography: p. 48.
1. Arctic Ocean. 2. Climate. 3. Cold regions. 4. Dynamics. 5. Ice. 6. Nonlinear mechanics. 7. Oceanography. 8. Plasticity. 9. Polar regions. 10. Pressure ridges. 11. Rheology. 12. Sea ice. I. United States. Army. Corps of Engineers. II. Cold Regions Research and Engineering Laboratory, Hanover, N.H. III. Series: CRREL Monograph 84-3.

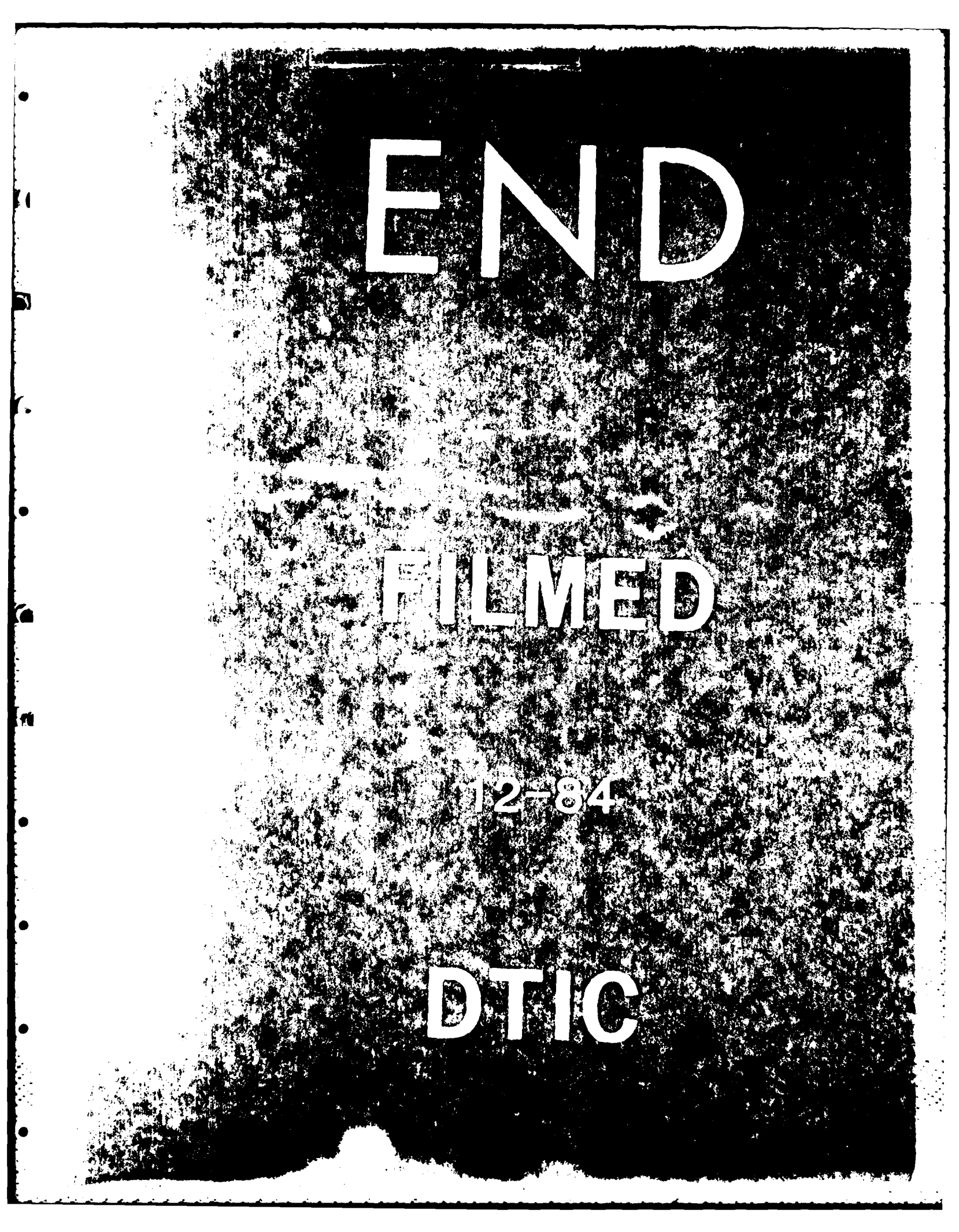
END
FILMED
12-84
DTIC